# 3 Results

## 3.1 The phylogenetic position of the Sericini

### Material and methods

*Taxon sampling*

This study included 49 taxa representing 48 genera, 24 tribes, 12 subfamilies of Scarabaeidae. Character coding was based on 92 species belonging to 66 genera (see appendix A 3.1). For several genera, particularly the larger ones such as *Aphodius*, *Maladera*, or *Serica*, more than one species was scored. For the elaboration of character systems not previously utilized for cladistic analysis, such as structures of mesendosternites or elytral base, many additional genera of this superfamily have been examined to assess variation within these structures.

The outgroup, *Trox sabulosus* (Trogidae), was chosen based on the phylogenetic hypothesis of the Scarabaeoidea proposed by Browne and Scholtz (1999). This taxon was also a basal Scarabaeoidea lineage in several other previous studies (e.g. Browne and Scholtz 1996, 1999; Howden 1982), and is certainly not part of the Scarabaeidae clade (Browne and Scholtz 1998). The choice of the taxa included into ingroup was mainly based on present and historical classification of the Sericini (e.g. Lacodaire 1856; Dalla Torre 1912) as well as on relationships discussed by previous authors (e.g. Browne and Scholtz 1998; Iablokov-Khnzorian 1977; Machatschke 1959; Nikolaev 1998; Sanmartin and Martin-Piera 2003). Hence, all to Sericini potentially closer related major lineages of Scarabaeidae were considered. Additionally, two taxa (*Aphodius* and *Copris*) were included as a test for an adequate outgroup choice as representatives of the well supported hypothetical sister clade of the 'melolonthine subgroup' plus Orphninae based on the tree of Browne and Scholtz (1998, Fig. 2).

*Characters*

One hundred and seven characters were coded, including 102 characters from the adult stage: head and its appendages (21), thoracic (3) and abdominal sclerites (4), legs (20), elytral base (7), posterior wing venation (7), endosternites (17), thoracic musculature (4), male (14) and female genitalia (5). Five characters were coded from immature stages (larval instar III). Data on larval morphology were taken from Giljarov (1964), Lumaret and Tauzin (1992), Medvedev (1952a), Paulian and Lumaret (1982), Klausnitzer and Krell (1996), Ritcher (1966), and McQuillan (1985), data on thoracic musculature based mainly on Larsén (1966). The wing venation nomenclature used herein follows Kukalová-Peck and Lawrence (1993). Of these 107 characters, 70 were binary and 37 multistate, and all were unordered. The character states are illustrated in Figs 17 - 28.

*Phylogenetic analysis*

The 107 morphological characters had a total of 261 states. Inapplicable characters were coded as "-", while unknown character states were coded as "?" (Strong and Lipscomb 1999). All characters were run equally weighted and nonadditive. The parsimony analysis was performed in NONA 2.0 (Goloboff 1999) using the parsimony ratchet (Nixon 1999) implemented in NONA and run in WINCLADA vs. 1.00.08 as a shell program (Nixon 2002). Two hundred iterations were performed (one tree hold per iteration). The number of characters to be sampled for reweighting during the parsimony ratchet was determined to be 10. All searches were run under the collapsing option "ambiguous" which collapses every node whose minimum length is 0. State transformations were considered to be apomorphies of a given node only if they were unambiguous (i.e., without arbitrary selection of accelerated

or delayed optimization) and if they were shared by all dichotomised most parsimonious trees. Bremer support (Bremer 1988, 1994) and parsimony jackknife (Farris et al. 1996) were evaluated using NONA. The search was set to a Bremer support level of 12, with seven runs (each holding a number of trees from 100 to 500 times multiple of suboptimal tree length augmentation) and a total hold of 8000 trees. The jackknife value was calculated running 100 replications with 100 search steps (mult*N) having one starting tree per replication (random seed 0). Character changes were mapped on the consensus tree using WINCLADA.

*Characters and character states*

In describing character states, I refrained from formulating any hypothesis about their transformation. In particular, coding is not implying, whether a state is derived or ancestral. The data matrix is presented in the appendix B 3.1.

*Adult*

*Head*

1. *Clypeus and labrum*: (0) separated by a suture (Figs 17A, 21A,C,D); (1) fused (Figs 17B, 21B) (ci: 0.50, ri: 0.94).

In the ground pattern of Coleoptera and of Scarabaeoidea, clypeus and labrum are separated (Matsuda 1965). Both are fused in *Pachypus*, Ablaberini, Sericini, and *Diphucephala*. While the labrum is strongly reduced in size in *Pachypus* (Fig. 21E), *Diphucephala* is characterized by a distinct sexual dimorphism affecting the labrum and its fusion with the clypeus where the labrum of the female is usually separated by a distinct suture while the separating suture may be completely reduced in the male.

2. *Lateral margin of clypeus and labrum*: (0) discontinuous (Figs 21A, B, C); (1) continuous (Figs 17A,B) (ci: 0.33, ri: 0.88).
3. *Clypeus anterior of eyes*: (0) not deeply sinuate (Figs 17A, 21A,B,G); (1) deeply sinuate (Fig. 21F) (ci: 1.0, ri: 1.0).
4. *Labrum*: (0) subequal in size to clypeus (Figs 17A,B, 21A-C); (1) distinctly smaller than clypeus (Figs 21D,E) (ci: 1.0, ri: 1.0).

The morphology of labrum varies considerably among Scarabaeoidea (Nel and De Villiers 1988; Nel and Scholtz 1990), soft tissue feeders such as Aphodiinae and Scarabaeinae and others such as Cetoniinae have a moveable membraneous labrum covered dorsally by the clypeus. All these taxa are considered to have character state 0.

5. *Number of antennomeres*: (0) nine or ten; (1) eight (ci: 0.14, ri: 0.14).

Krell (1992) discussed the morphogenesis of antenna and the teratological fusion of antennomeres within Scarabaeidae evaluating the practicability of the number of antennomeres as a character for phylogenetic systematics. Due to a certain evolutionary trend of fusion of antennomeres, the homoplasy of the character is expected to be high. In species of several sericine genera, the number of antennomeres is both, either nine or ten. To remove this "noise" from cladistic analysis, antenna with nine or ten antennomeres were coded as one character state (0).

6. *Number of teeth of galea*: (0) six; (1) seven; (2) eight (Fig. 17E); (3) without any tooth (Figs 17C,J,K); (4) five (Figs 17D,F) (ci: 0.44, ri: 0.80).
7. *Galea*: (0) with a distal movable tooth separated from the galea by a thin membrane (Fig. 17F); (1) all teeth completely fused with the galea (Fig. 17D); (2) with two separate tooth-like spines (Fig. 17G); (3) without teeth, finely setose (Fig. 17K); (4) without teeth, very robustly and finely setose (Fig. 17J); (5) with a distal, movable tooth separated from the galea by an incomplete suture (ci: 0.62, ri: 0.83).


**Fig. 17. A:** head, cranial view: *Phyllotocus macleayi*; **B:** labroclypeus, cranial view: *Calloserica langtangica*; **C:** maxilla, medioventral view: *Pachypus candidae*; **D:** galea of maxilla, medioventral view: *Heteronyx* sp.; **E:** galea of maxilla, mesomedial view: *Paratriodonta romana*; **F:** maxilla, ventral view: *Diphucephala* sp.; **G:** galea of maxilla, ventral view: *Hoplia graminicola*; **H:** lacinia and dorsal process of parastipes (maxilla), medial view: *Sparrmannia* sp.; **J:** galea of maxilla, mesomedial view: *Orphnus* sp.; **K:** galea of maxilla, mesomedial view: *P. macleayi*; **L:** maxilla, medial view: *Maladera holosericea*; **M:** maxilla, medial view: *Cyrtocamenta pygidialis*; **N:** maxilla, medial view: *Telura alta*; **O:** galea of maxilla, medial view: *Hymenochelus distinctus*; **P:** galea of maxilla, ventral view: *H. distinctus*; **Q:** maxilla, medial view: *Chasmatopterus hirtus*; **R:** maxilla, medial view: *Omaloplia spireae*; **S:** maxilla, medial view: *Diphucephala* sp.; **T:** labium, medial view: *Gastroserica marginalis*; **U:** labium, medial view: *C. pygidialis*; **V:** labium, ventrolateral view: *O. spireae*; **W:** labium, ventrolateral view: *Pachyserica olafi*. Scale: G, N, O: 30 µm; A - F, H - M,P - W: 100 µm.

It seems not reasonable to regard the distal movable tooth of the galea as homologous with the distogalea. The larvae of the taxa in question (*Diphucephala*, *Sericoides*, *Telura*) have a galea with only one joint. Since the distogalea in Coleoptera does not posses musculature, it is difficult to prove this argument by examination of the maxillary musculature. Character state 2 is only known from Hopliinae (*Hoplia*) and *Phaenomeris*.

8. *Dorsal process of mediostipes apically*: (0) not widened (Figs 17L,N,R,S); (1) widened (Fig. 17M); (2) absent (Fig. 17Q); (3) enlarged and widely fused with lacinia and mediostipes (Fig. 17H) (ci: 0.37, ri: 0.73).

The nomenclature of the relevant maxillary sclerites is based on Williams (1938) and Beutel (1994). Nel and Scholtz (1990) used the term parastipes for this sclerite, while they used "latero-stipes" for the palpifer being misled by the strongly developed basal palpifer in Scarabaeidae (see Figs 17L,M).

9. *Galea*: (0) with basal and distal joint (Fig. 17J); (1) with one joint only (Figs 17G,H,K) (ci: 1.0, ri: 1.0).
10. *Number of teeth on galea (visible in ventral view)*: (0) four; (1) three (ci: 0.20, ri: 0.69).
11. *Dorsal and ventral row of galeal teeth*: (0) on the same level (Figs 17E,M,N,R); (1) dorsal row basally, ventral row distally displaced (Fig. 17J) (ci: 1.0, ri: 1.0).
12. *Lacinia distally*: (0) long, reaching the teeth of galea, but not fused with galea basally (Fig. 17N); (1) short, reaching at most the base of the galea (Figs 17L,M); (2) long, reaching the teeth of the galea, fused with galea basally (Fig. 17Q) (ci: 0.28, ri: 0.50).

The lacinia in Adephagan Coleoptera and in most Polyphaga (including basal Scarabaeoidea) is long (e.g. Beutel 1997; Hansen 1997; Nel and Scholtz 1990).

13. *Lacinia basally*: (0) not shortened (Figs 17L,M,N); (1) shortened (Figs 17Q,R,S); (2) lacinia absent (Fig. 17C) (ci: 0.40, ri: 0.40).
14. *Stipes*: (0) almost twice as long as wide (Fig. 21J); (1) stout, at most little longer than wide (Fig. 21H) (ci: 0.33, ri: 0.50).
15. *Mentum*: (0) wider than ligular lobes combined (Fig. 21T); (1) as wide as ligular lobes combined or narrower (Figs 21S,U,V) (ci: 0.10, ri: 0.60).

The terminology of labial appendages suffers from ambiguous homology assessments. Although the mentum was interpreted by Snodgrass (1932, 1935) and Anderson (1936) as the basal division of the prementum, workers since Das (1937) have correctly interpreted the area as the mentum (Matsuda 1965). Most authors apply the term ligula for medially fused paraglossal lobes (e.g. Snodgrass 1932, 1935) or as a collective term for all labial lobes (e.g. Snodgrass 1935). Assuming that the median fusion of paraglossae evolved more than once in Coleoptera, the term "ligula", in the first case, might consequently describe a non-homologous structure. The labium of scarabeid larvae do not present either glossae or paraglossae sometimes have a simple ligula (Ritcher 1966). Ligular muscles, such as the flexor muscle of the glossa or the flexor muscle of the paraglossa in *Periplaneta* (Dorsey 1943), are not present in Coleoptera (Matsuda 1965). Nel and Scholtz (1990) used the term "ligular lobes" (inner/ outer) of Snodgrass (1935) to describe the lobe-shaped appendages of the prementum without assessing homology. However, the presence of very small "glossae" in the quadrilobed ligular type (present in some Scarabaeinae) does not contradict the hypothesis (Crampton 1928) that in Coleoptera the widely distributed bilobed ligular type (see e.g. Williams 1938) is composed in widest part by the more or less completely fused paraglossae. Consequently, I assume homology of the ligular lobes in the bilobed ligular type within Scarabaeidae. It should be taken into consideration that a stronger sclerotization of the linking membrane between the prementum and the ligular lobes might produce a similar "ligula"-like median structure, without that the lateral ligular lobes are reduced or any portion of a glossa must have been involved.

16. *Palpiger and prementum*: (0) separate by a suture (Figs 17V, 18G); (1) fused (without a visible suture) (Figs 17W, 18B,E,F); (2) widely separate by a membrane (Fig. 18A) (ci: 0.14, ri: 0.73).

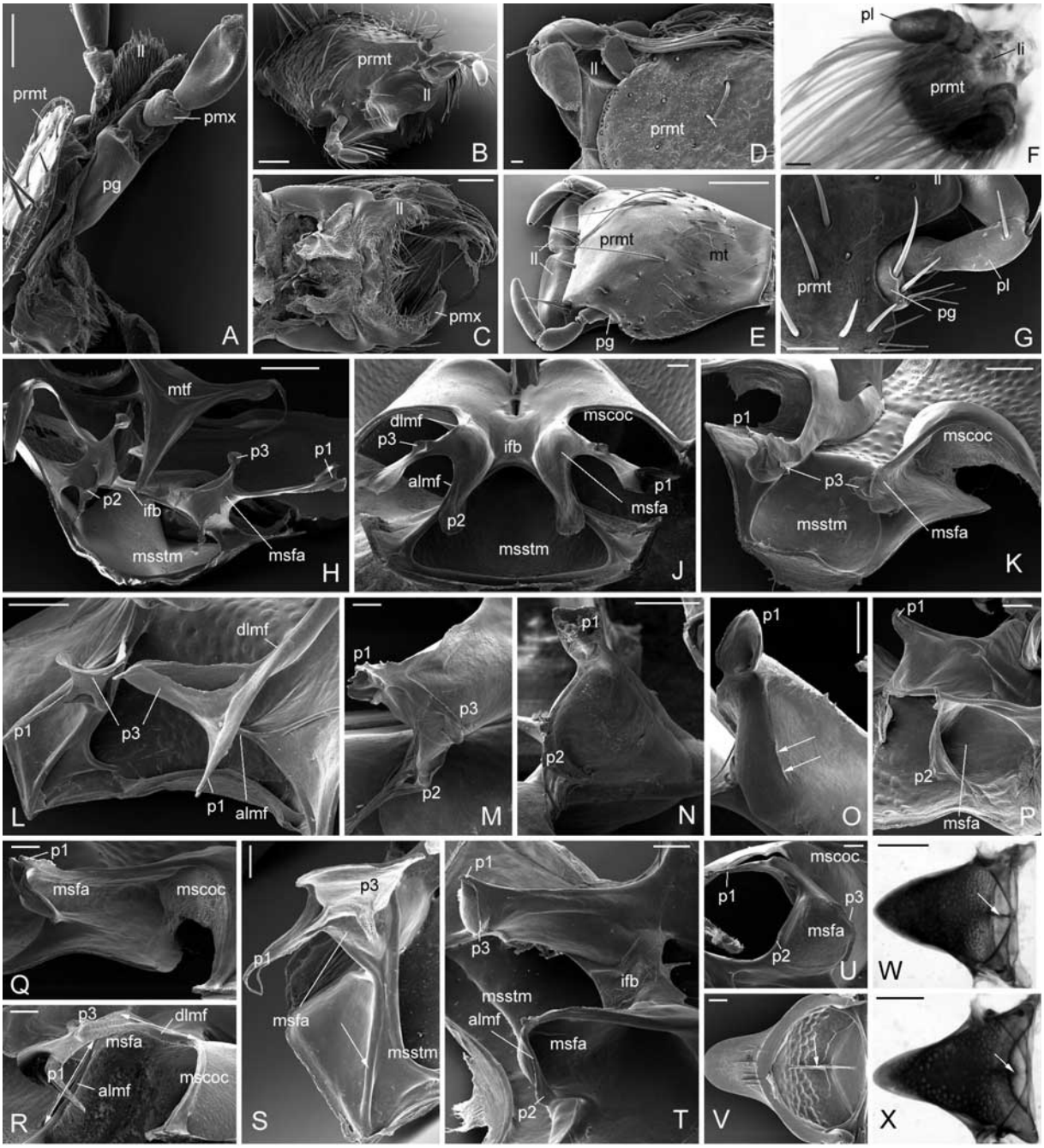


**Fig. 18. A:** labium, ventrolateral view: *Phyllotocus macleayi*; **B:** labium, ventrolateral view: *Adoretus* spec.; **C:** labium, medial view: *Chasmatopterus hirtus*; **D:** craniolateral portion of the labium, ventral view: *Diphucephala* spec.; **E:** labium, ventrolateral view: *Trochalus* sp.; **F:** labium, cranial view: *Pachypus candidae*; **G:** craniolateral portion of the labium, ventral view: *Sericoides* sp.; **H:** mesofurca and metafurca, cranial view: *Anaplotrupes stercorosus*; **J:** mesofurca, cranial view: *Aphodius scrutator*; **K:** mesofurca, craniolateral view: *Hymenoplia castilliana*; **L:** mesofurca, craniolateral view: *Maladera holosericea*; **M:** mesofurca, craniolateral view: *Anisoplia segetum*; **N:** mesofurcal arm, craniolateral view: *Pseudopanotrogus clypealis*; **O:** mesofurca, craniolateral view: *Potosia cuprea*; **P:** mesofurca, lateral view: *P. macleayi*; **Q:** mesofurca, lateral view: *H. castilliana*; **R:** mesofurca, lateral view: *A. scrutator*; **S:** mesofurcal arm, cranial view: *Maladera holosericea*; **T:** mesofurca, lateral view: *Raysymmela pallipes*; **U:** mesofurcal arm, cranial view: *Onthophagus* spec.; **V:** mesonotum, medial view: *R. pallipes*; **W:** mesonotum, medial view: *Omaloplia spireae*; **X:** mesonotum, medial view: *Sericania fuscolineata*. Scale: D, F: 20 µm; A, C, G, M, N, P, Q, S - V: 100 µm; B, E, J, K, L, R: 200 µm; O: 300 µm; W, X: 500 µm; H: 1 mm.

17. *Palpiger and ligular lobes*: (0) separate (Figs 17W, 18A,D,E,G); (1) fused (without a visible suture) (Figs 17V, 18B,F) (ci: 0.14, ri: 0.73).
18. *Palpiger*: (0) not enclosed by prementum and ligular lobe (Fig. 18A); (1) enclosed by

prementum and ligular lobe (Figs 18B,D,E,F,G) (ci: 0.50, ri: 0.75).

19. *Palpiger or its homologous equivalent (in ventral view)*: (0) visible (Figs 17V,W, 18A,B,D,E,G); (1) not visible (Figs 17T,U, 18D,F) (ci: 0.09, ri: 0.28).
20. *Prementum and ligular lobe*: (0) separate by a suture (Figs 17V,W, 18A,D,E); (1) fused (without visible suture) (Figs 18B,F,G) (ci: 0.14, ri: 0.72).
21. *Ligular lobes*: (0) separated (at least by a suture) (Figs 17V, 18A,C,D,E); (1) fused with each other (Figs 17W, 18B); (2) fused but strongly reduced in size to a small median ligular lobe (Fig. 18F) (ci: 0.25, ri: 0.68).

*Thorax*

22. *Hypomeron (prothorax) basiventrally*: (0) without transverse carina (Figs 21K,L); (1) with transverse carina (Fig. 21M) (ci: 0.50, ri: 0.50).

The pronotum of Coleoptera is large and it extends to the ventral surface of prothorax (Crampton 1926; Beutel and Haas 2000). The derivation of ventral prothoracic portion was long debated (Matsuda 1970). While Ritcher (1969) stated for Scarabaeoidea that "the true origin of the epimeron [= hypomeron] as a pleural element", current hypothesis is that, in Polyphagan beetles, the propleuron is reduced in length and width (Hlavac 1975) and that is internalised and fused with the trochantinus (Beutel 1997; Beutel and Haas 2000).

23. *Edge of intersegmental membrane at the basis of pronotum medially (ventral view)*: (0) present and elevate (Fig. 21K); (1) absent (Figs 21L,M) (ci: 0.50, ri: 0.88).
24. *Pronotum, basal marginal line*: (0) present; (1) absent (ci: 0.10, ri: 0.18).

A rather variable character which is apparently more informative at lower taxonomic levels.

25. *Mesofurcal arm, anterior lamina*: (0) as long as dorsal lamina (Fig. 21Q); (1) shorter than dorsal lamina (Figs 21N,S); (2) longer than dorsal lamina (Figs 21P,R) (ci: 0.50, ri: 0.33).
26. *Mesofurcal arm, interior process (p3)*: (0) small (Figs 18J,T); (1) large (Figs 18K,L) (ci: 1.0, ri: 1.0).
27. *Mesofurcal arms*: (0) joined by a median sclerotized bridge (Figs 18J,T); (1) separate, without median bridge (Figs 18K,L) (ci: 0.20, ri: 0.73).
28. *Mesofurca and mesosternum, carina from craniolateral margin of mesosternum to mesofurcal arm*: (0) absent (Figs 18H,J,K,T); (1) present (Figs 18L,S) (ci: 1.0, ri: 1.0).
29. *Mesofurcal arm, craniomedial surface*: (0) large and convex (Figs 18H,J,K,O,P,T); (1) small and conical (Figs 18K,L,N); (2) narrow and long (Fig. 18U) (ci: 0.50, ri: 0.83).
30. *Mesofurcal arm, dorsal lamina*: (0) without fringe (Figs 18H-U, 21O-S); (1) with a membraneous fringe (Fig. 21N) (ci: 1.0, ri: 1.0).
31. *Mesofurcal arm, dorsal process (p1)*: (0) very long and reflexed (Figs 18J,U, 21R); (1) short and straight (Figs 18K-P,Q,T, 21N,S); (2) very short (Figs 21O-Q) (ci: 0.33, ri: 0.33).
32. *Mesofurcal arm, dorsal process (p1) apically*: (0) widened (Figs 18H,J,R, 21N,R); (1) narrowed (Figs 18K-P,Q,T, 21N,S); (2) medially widened, in apical portion laterally produced, with acute apex (Fig. 18U) (ci: 0.50, ri: 0.33).
33. *Mesofurcal arm, anterior process (p2)*: (0) present (Figs 18H,J,M,O,P,T,U); (1) absent (Figs 18K,L,N,S) (ci: 0.33, ri: 0.83).
34. *Mesofurcal arm, interior process (p3)*: (0) shape lobiform (Figs 18K,L,M,N,S); (1) shape fringe-like (Figs 18O,U); (2) absent (Fig. 18P) (ci: 0.22, ri: 0.74).
35. *Mesofurcal arm, anterior process (p2)*: (0) separate from anterior lamina (Figs 18J,M); (1) fused with anterior lamina of mesofurca (Fig. 18N) (ci: 0.50, ri: 0.66).
36. *Median keel of mesonotum (medial view)*: (0) present (Figs 18V,W); (1) absent (Figs 18X) (ci: 0.16, ri: 0.58).

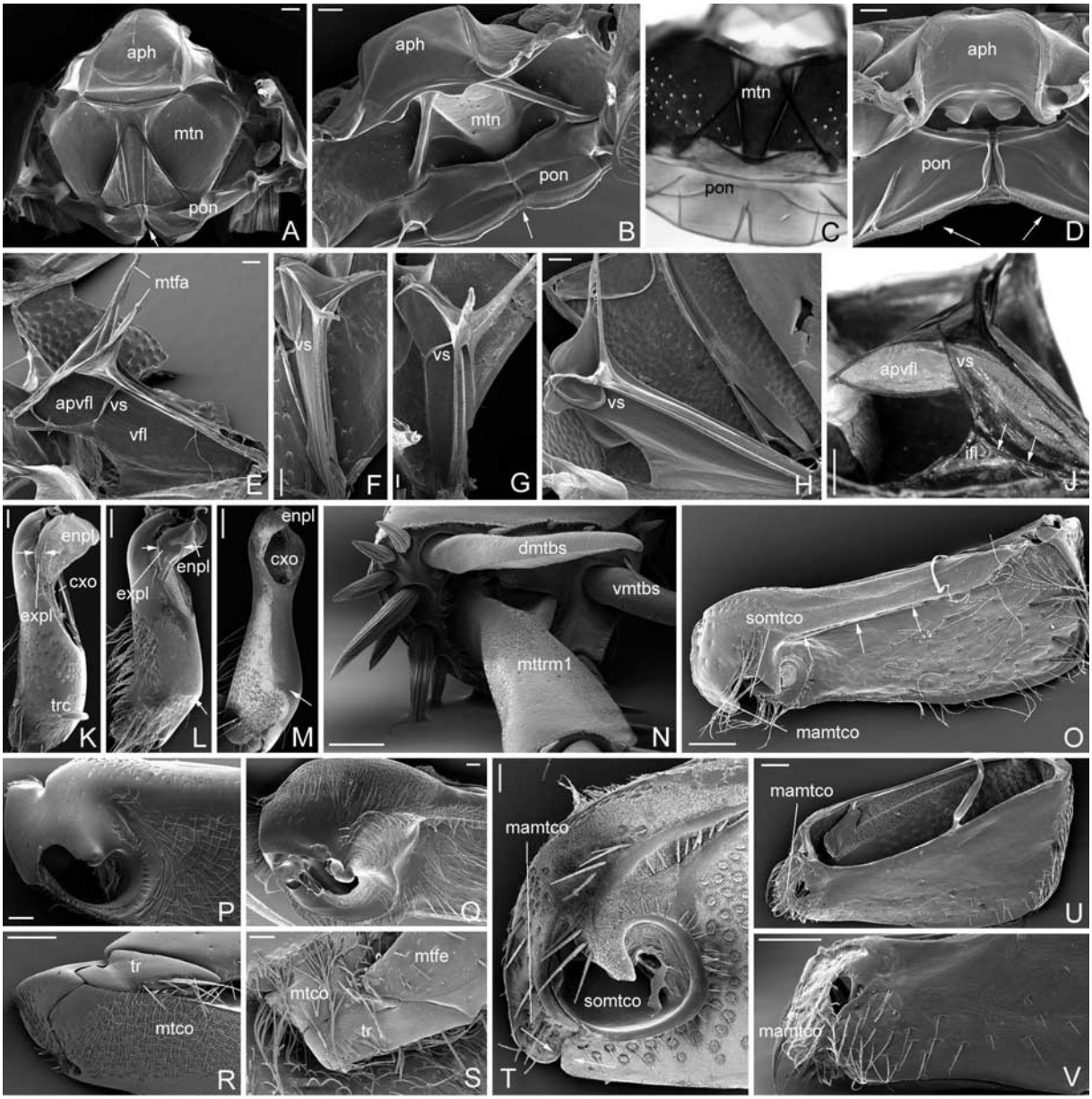


**Fig. 19. A:** metanotum, medial view: *Pseudopanotrogus clypealis*; **B:** metanotum, cranial view: *Hymenoplia castilliana*; **C:** metanotum, medial view: *Chasmatopterus hirtus*; **D:** metanotum, cranial view: *Athlia rustica*; **E:** metafurca, lateral view: *C. hirtus*; **F:** metafurca, lateral view: *Phyllotocus macleayi*; **G:** metafurca, lateral view: *Camenta westermanni*; **H:** metafurca, lateral view: *Maladera holosericea*; **J:** metafurca, lateral view: *Propomacrus mucronatus*; **K:** procoxa, cranial view: *P. clypealis*; **L:** procoxa, cranial view: *H. castilliana*; **M:** procoxa, medial view: *M. holosericea*; **N:** metatibia, apical view: *Pleophylla* sp.; **O:** metacoxa, ventral view: *C. hirtus*; **P:** metacoxa apical portion, ventral view: *Potosia cuprea*; **Q:** metacoxa apical portion, ventral view: *Geotrupes stercorosus*; **R:** metacoxa apical portion, caudoventral view: *Onthophagus fracticornis*; **S:** metacoxa apical portion, ventral view: *Diphucephala* sp.; **T:** metacoxa apical portion, ventral view: *M. holosericea*; **U:** metacoxa, medial view: *H. castilliana*; **V:** metacoxa, caudal view: *H. castilliana.* Scale: B, E, J, N, S, T: 100 µm; D, F - H, K, L, O, Q, R, U, V: 200 µm; A,M,P: 300 µm.

37. *Caudal lobes of postnotum (metathorax)*: (0) long and narrow (Fig. 19A); (1) short and wide (Figs 19B,C); (2) reduced (Fig. 19D) (ci: 0.50, ri: 0.90).
38. *Incision between caudal lobes of postnotum (metathorax)*: (0) deep (Fig. 19A); (1) small or absent (Figs 19B,C,D) (ci: 0.25, ri: 0.85).
39. *Anterior and posterior margin of ventral median flange of metendosternite (lateral view)*: (0) convergent toward base or subparallel (Figs 19F,G); (1) evenly divergent toward base (Figs 19E,H); (2) extremely divergent in basal half (Fig. 19J) (ci: 0.33, ri: 0.85).

The terminology of metendosternite is based on Crowson (1944), with reference to de Castro

(2001). The strongly divergent anterior and posterior margin of ventral median flange of metendosternite is supported by the interiorly strongly produced internal flange of metasternal longitudinal suture, which closely attaches to the ventral median flange. Both flanges may be completely or partly fused (with a visible suture, Fig. 19J, arrows).

40. *Metafurca, apical portion of ventral median flange (portion apical of ventral suture, lateral view)*: (0) short (shorter than the furcal arm) (Figs 19F,G,H); (1) long (as long as the furcal arm, or longer) (Figs 19E,J) (ci: 0.33, ri: 0.85).

Pretorius et al. (2000) noticed that in Scarabaeinae the size of the ventral median flange is reduced in flightless taxa.

41. *Metafurca, apex of ventral median flange (portion apical of ventral suture, lateral view)*: (0) rounded (Figs 19F,G,H); (1) acutely pointed (Figs 19E,J) (ci: 0.25, ri: 0.78).

*Musculature of thorax* (nomenclature according to Larsén 1966)

The thoracic musculature of Scarabaeoidea has been studied in some detail by Larsén (1966). For a number of taxa I could examine the thoracic musculature, however, not for all taxa included into the analysis suitable material was available to examine thoracic musculature characters. Nevertheless these characters are important in order to interpretate functional relationships to skeletal characters and to reconstruct the groundplan of principle phytophagous scarab lineages.

42. *M37 (M. furco-pleuralis)*: (0) present; (1) absent (ci: 1.0, ri: 1.0).
43. *M49 (M. epimero-trochanteralis)*: (0) present; (1) absent (ci: 1.0, ri: 1.0).
44. *M52 (M. furca-trochanteralis)*: (0) present; (1) absent (ci: 1.0, ri: 1.0).
45. *M78 (M. coxa-basalaris)*: (0) present; (1) absent (ci: 1.0, ri: 1.0).

*Legs*

46. *Ratio of length of metepisternum/ metacoxa*: (0) greater than or subequal to 1.0 (Fig. 22G); (1) smaller than 1.0 (Fig. 22H) (ci: 0.50, ri: 0.92).
47. *Ostium of procoxa*: (0) large (at least half as long as the procoxal length) (Figs 19K,L); (1) small (distinctly less than half as long as procoxal length) (Fig. 19M) (ci: 1.0, ri: 1.0).
48. *Procoxa, transversal carina*: (0) present (Fig. 19K); (1) absent (Figs 19L,M) (ci: 0.20, ri: 0.71).

The transversal carina and a furrow in the prosternum form a secondary coxo-sternal articulation that fixes the coxa more firmly in its longitudinal rotational axis.

49. *Fusion of the proexopleura and trochantin*: (0) narrow (Fig. 19K); (1) wide (Figs 19L,M) (ci: 1.0, ri: 1.0).

The propleuron is motile and attached to notum at level of the dorsal wall (Hlavac 1975). It rotates, along with the coxa, around a notal condyle. The endopleuron is shifted anteriorly so that most of it is anterior to than above the exopleuron. The exo- and endopleura are developed ventrally resulting in the reduction of the trochantin (Hlavac 1975).

50. *Mesocoxae*: (0) contiguous, not separate by mesosternum (Fig. 21T); (1) separate by mesosternum (Fig. 21U); (2) very widely separate by mesosternum (Fig. 21V) (ci: 0.40, ri: 0.72).
51. *Apex of mesotibia*: (0) with two principal spines (Fig. 22R); (1) with the medial principal spine absent (Fig. 22Q); (2) without principal spines (ci: 1.0, ri: 1.0).

The homology of the principal spines may be concluded based on an examination of the structure of their surface, which is transversely scale-like in principal spines but longitudinally scratched in the remainder of robust setae of the apical face of the tibia.

52. *Metacoxa*: (0) basally narrowed (Figs 22A,B); (1) basally widened with the posterior margin produced posteriorly at base (Figs 22C-F) (ci: 1.0, ri: 1.0).

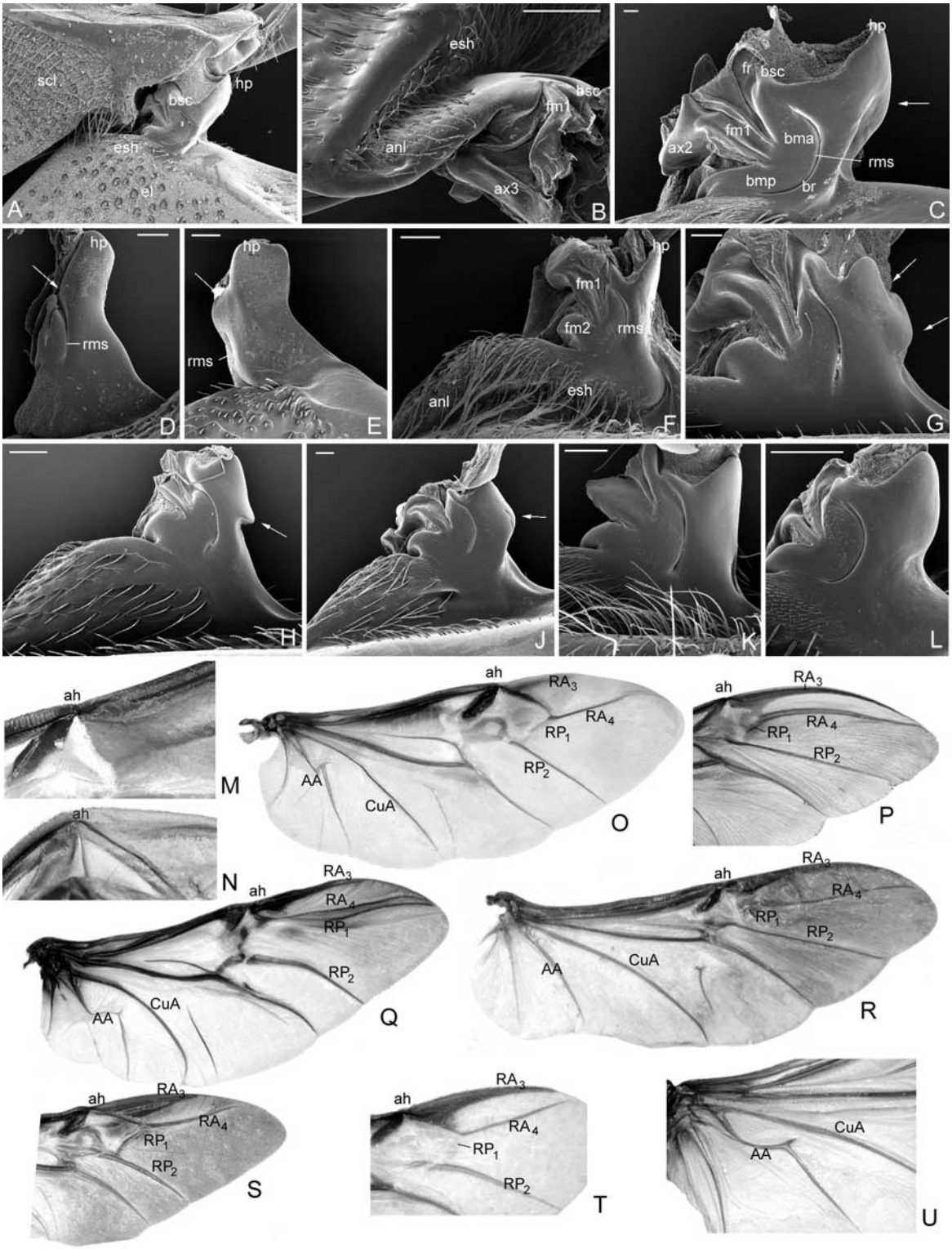


**Fig. 20. A:** elytral-scutellar articulation, dorsal view: *Maladera holosericea*; **B:** elytral basis, mesodorsal view: *Adoretus* sp.; **C:** elytral basis, dorsal view: *M. holosericea*; **D:** elytral basis, dorsal view: *Valgus hemipterus*; **E:** elytral basis, dorsal view: *Potosia cuprea*; **F:** elytral basis, dorsal view: *Pachypus candidae*; **G:** elytral basis, dorsal view: *Camenta westermanni*; **H:** elytral basis, dorsal view: *Orphnus* sp.; **J:** elytral basis, dorsal view: *Raysymmela pallipes*; **K:** elytral basis, dorsal view: *Melolontha melolontha*; **L:** elytral basis, dorsal view: *Hymenoplia castilliana*; **M:** ala, cranial margin, dorsal view: *Osmoderma eremita*; **N:** ala, cranial margin, dorsal view: *C. westermanni*; **O:** ala, dorsal view: *Maladera simlana*; **P:** ala, apical portion, dorsal view: *Propomacrus mucronatus*; **Q:** ala, dorsal view: *Aphodius scrutator*; **R:** ala, dorsal view: *Tropinota hirta*; **S:** ala, apical portion, dorsal view: *Hoplia graminicola*; **T:** ala, apical portion, dorsal view: *Acoma* sp.; **U:** ala, basal portion, dorsal view: *P. mucronatus*. Scale: C: 20 µm; J: 30 µm; D, G, H, L: 100 µm; A, B, E, F, K: 200 µm, M – U: not to scale.

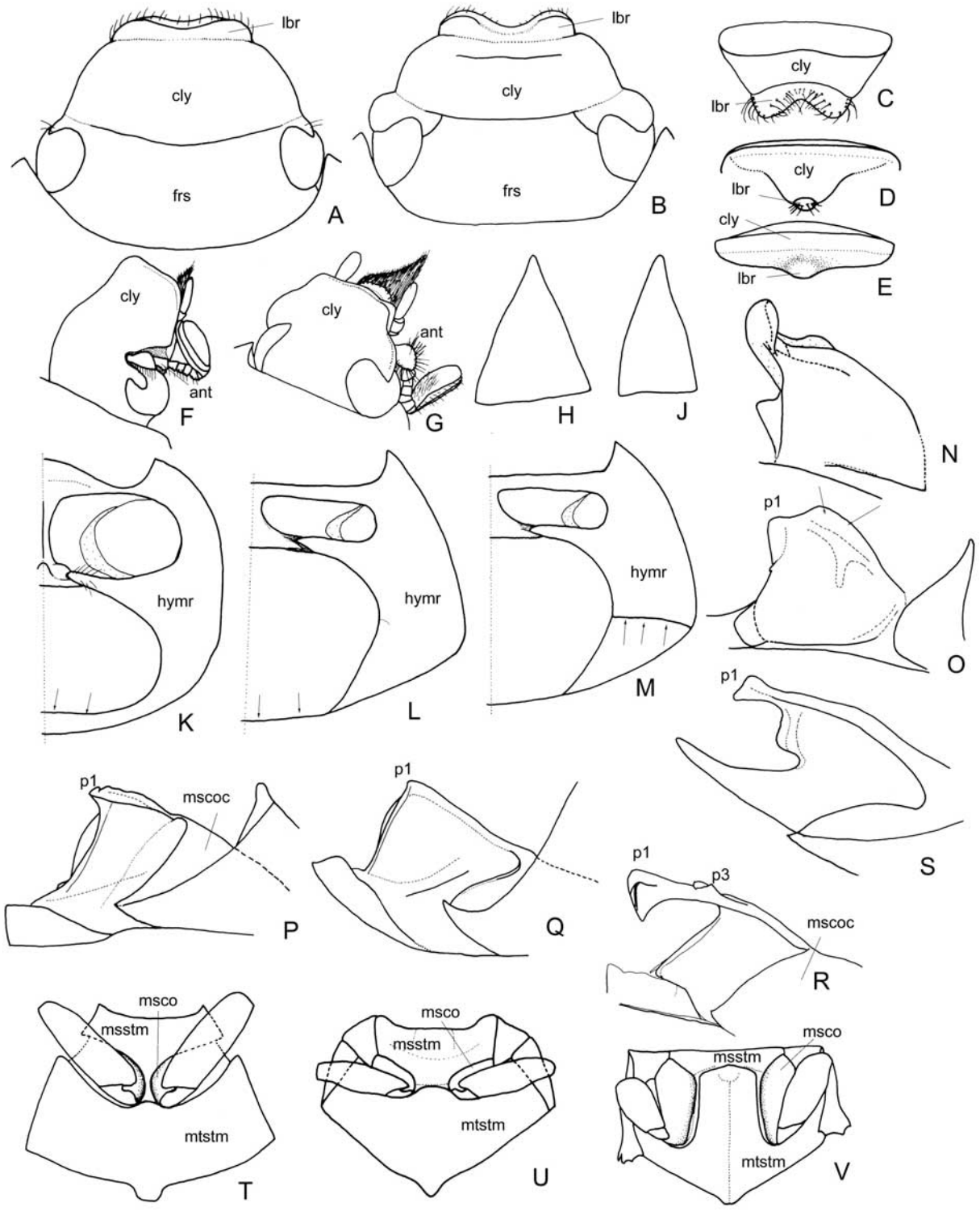


**Fig. 21. A:** head, dorsal view: *Athlia rustica*; **B:** head, dorsal view: *Camenta westermanni*; **C:** labrum, cranial view: *Melolontha melolontha*; **D:** labrum, cranial view: *Europteron gracile*; **E:** labrum, cranial view: *Pachypus candidae*; **F:** head, dorsolateral view: *Potosia cuprea*; **G:** head, dorsolateral view: *Propomacrus mucronatus*; **H:** stipes (maxilla), ventral view: *M. melolontha*; **J:** stipes (maxilla), ventral view: *Maladera holosericea*; **K:** prothorax, ventral view: *E. gracile*; **L:** prothorax, ventral view: *Hyposerica* sp.; **M:** prothorax, ventral view: *Maladera simlana*; **N:** mesofurca, lateral view: *P. cuprea*; **O:** mesofurca, lateral view: *Oryctes nasicornis*; **P:** mesofurca, lateral view: *Orphnus* sp.; **Q:** mesofurca, lateral view: *P. candidae*; **R:** mesofurca, lateral view: *Aphodius scrutator*; **S:** mesofurca, lateral view: *M. melolontha*; **T:** pterothorax, ventral view: *Adoretus* sp.; **U:** pterothorax, ventral view: *Maladera renardi*; **V:** pterothorax, ventral view: *Copris lunaris* (not to scale).

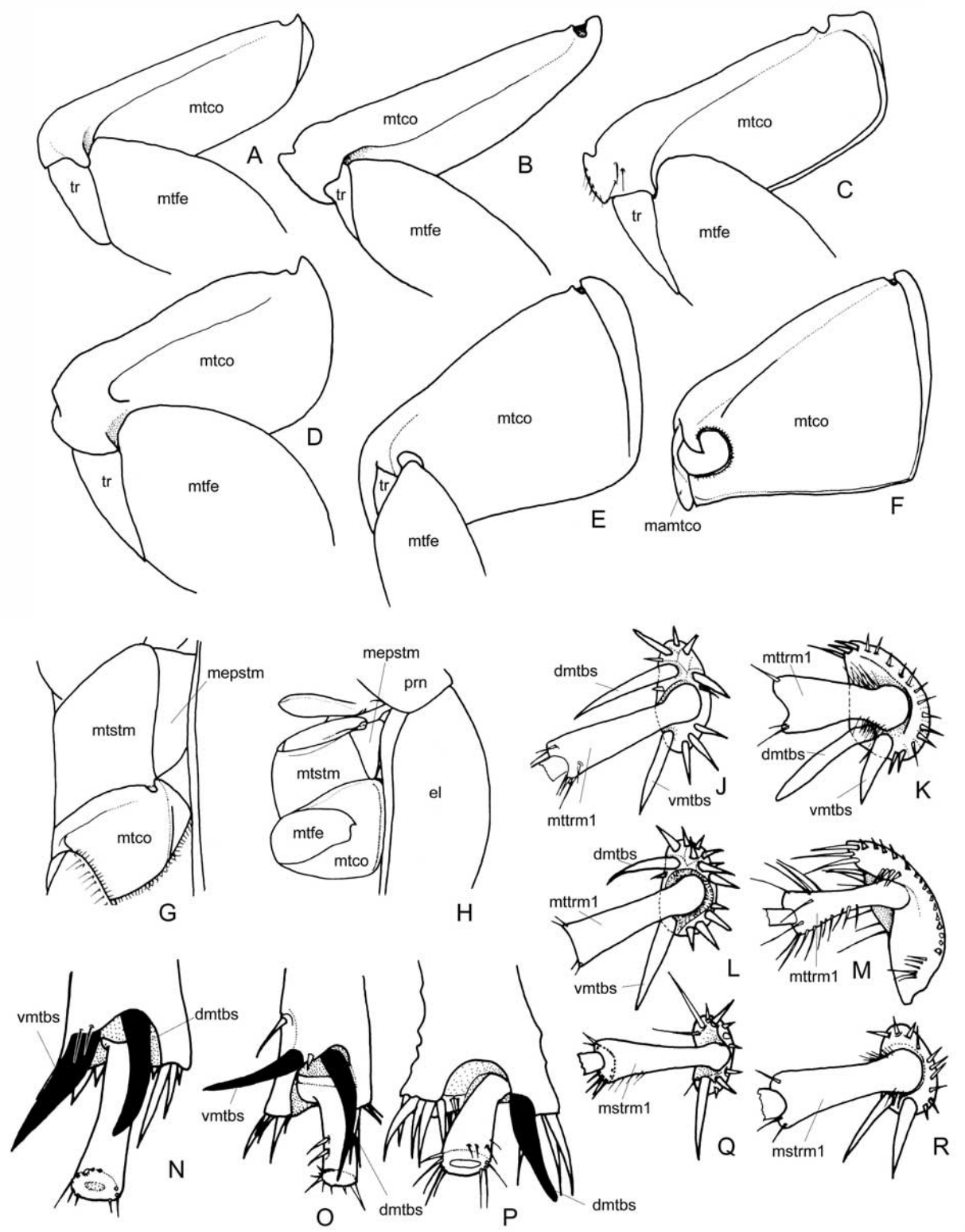


**Fig. 22. A:** metacoxa, ventral view: *Aphodius scrutator*; **B:** metacoxa, ventral view: *Catharsius molossus*; **C:** metacoxa, ventral view: *Propomacrus mucronatus*; **D:** metacoxa, ventral view: *Pachypus candidae*; **E:** metacoxa, ventral view: *Trochalus* sp.; **F:** metacoxa, ventral view: *Hyposerica* sp.; **G:** metasternum, lateral view: *Oryctes nasicornis*; **H:** metasternum, lateral view: *Maladera* sp.; **J:** metatibia, apical view: *Maladera renardi*; **K:** metatibia, apical view: *Melolontha melolontha*; **L:** metatibia, apical view: *Pleophylla* sp.; **M:** metatibia, apical view: *Diphucephala* sp.; **N:** metatibia, medial view: *Sericoides* sp.; **O:** metatibia, medial view: *Phyllotocus macleayi*; **P:** metatibia, medial view: *Diphucephala* sp., female; **Q:** mesotibia, apical view: *M. renardi*; **R:** mesotibia, apical view: *M. melolontha* (not to scale).

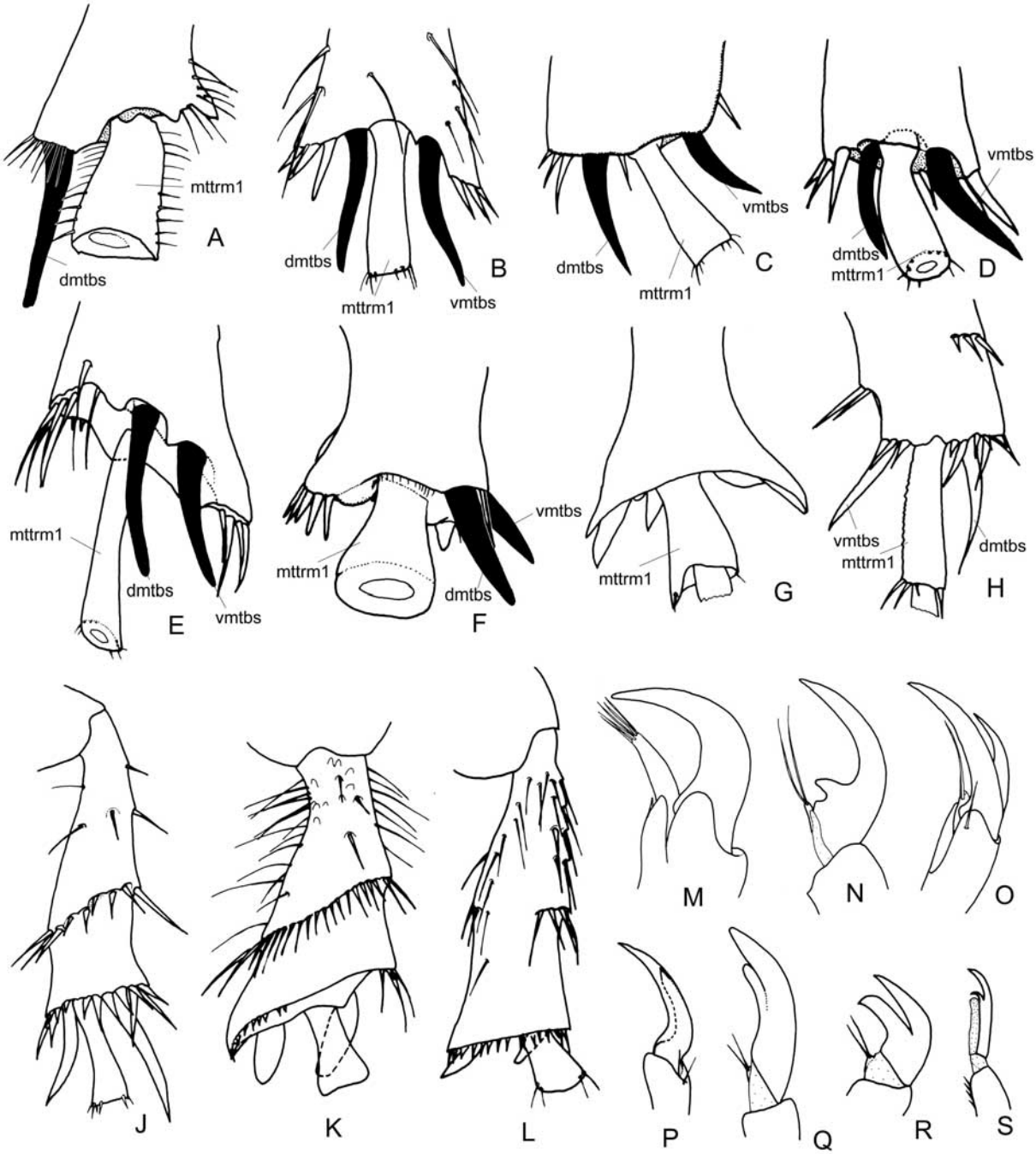


**Fig. 23. A:** apical portion of metatibia, medial view: *Catharsius molossus*; **B:** apical portion of metatibia, medial view: *Empecamenta buettikeri*; **C:** apical portion of metatibia, medial view: *Maladera insanabilis*; **D:** apical portion of metatibia, medial view: *Heteronyx* sp.; **E:** apical portion of metatibia, medial view: *Elaphocera* sp.; **F:** apical portion of metatibia, medial view: *Anisoplia segetum*; **G:** apical portion of metatibia, lateral view: *Propomacrus mucronatus*; **H:** apical portion of metatibia, lateral view: *M. insanabilis*; **J:** metatibia, lateral view: *Hybalus graecus*; **K:** metatibia, lateral view: *Pachypus candidae*; **L:** metatibia, lateral view: *Chasmatopterus hirtus*; **M:** metatarsal claw, lateral view: *Oryctes boas*; **N:** metatarsal claw, lateral view: *Melolontha melolontha*; **O:** metatarsal claw, lateral view: *Anisoplia segetum*; **P:** metatarsal claw, lateral view: *Hoplia graminicola*; **Q:** metatarsal claw, lateral view: *Cyrtocamenta pygidialis*; **R:** metatarsal claw, lateral view: *M. insanabilis*; **S:** metatarsal claw, lateral view: *Hymenochelus distinctus* (not to scale).

53. *Apex of metacoxa, medial apophysis*: (0) absent (Figs 19P-S, 22A-D); (1) present, produced posteriorly (Figs 19O,T-V, 22E,F) (ci: 0.12, ri: 0.46).
54. *Metacoxa, secondary ostium produced by medial apophysis and posterior margin of metacoxa*: (0) open (Figs 19O,U,V); (1) closed posteriorly (Figs 19T, 22E,F) (ci: 1.0, ri: 1.0).

55. *Metacoxa, marginal line of posterior margin*: (0) absent (Fig. 22E); (1) present (Figs 19O, 22C,F) (ci: 0.10, ri: 0.10).
56. *Metacoxa, marginal line of lateral margin*: (0) absent (Figs 22B,D); (1) present (Figs 19O, 22C,E,F) (ci: 0.50, ri: 0.75).
57. *Metacoxa, submarginal line of anterior margin*: (0) present (Figs 19O, 22A-D,F).; (1) absent (Fig. 22E) (ci: 0.50, ri: 0.50).
58. *Metatibia, interior setae on apical face*: (0) absent (Figs 22J,K); (1) robust (Fig. 22L); (2) fine (Fig. 22M) (ci: 0.33, ri: 0.60).
59. *Metatibia, transversal carina on lateral face*: (0) complete (from dorsal to ventral margin) (Figs 23J,K); (1) interrupted at middle (Fig. 23L) (ci: 0.33, ri: 0.60).
60. *Apex of metatibia (except of the principal spines)*: (0) with spines and / or setae (Figs 22J-M, 23H-L; (1) glabrous (Fig. 23G) (ci: 0.20, ri: 0).
61. *Apex of metatibia, principal spines*: (0) close to each other on medial face (subapical) in the middle of tibia (left and right side of tarsal articulation) (Figs 22N,O); (1) widely separated on medial or apical face (subapical or apical) of left and right side of tarsal articulation (Figs 23B-D); (2) ventrally and contiguously on apical face (Fig. 23F); (3) present with one ventroapical spine only (Figs 22P, 23A); (4) close to each other but separate on apical face, sublateral in respect to tarsal articulation (Fig. 23E) (ci: 0.40, ri: 0.73).
62. *Meso- and metatarsal claws*: (0) simple (Fig. 23M); (1) with a basal or median tooth ventrally (Figs 23N,R,S); (2) with a median lobe ventrally (Fig. 23Q); (3) not toothed ventrally but incised apically (Fig. 23O) (ci: 0.37, ri: 0.75).
63. *Tarsal claws ventrally*: (0) without membranous fringe (Figs 23M-R); (1) with membranous fringe (Fig. 23S) (ci: 1.0, ri: 1.0).
64. *Meso- and metatarsal claws*: (0) symmetrical (Figs 23M,N,Q-S); (1) asymmetrical (Figs 23O,P) (ci: 0.50, ri: 0.66).
65. *Meso- and metatarsal claws*: (0) immotile (Figs 23M,N,Q-S); (1) motile (Figs 23O,P) (ci: 0.50, ri: 0.66).

*Elytra*

66. *Elytral shelf*: (0) on a lower level in contrast to elytral surface (Figs 20B,J,K); (1) on the same level as the elytral surface (Figs 20A,C) (ci: 1.0, ri: 1.0).

The transverse groove separating the mesoscutum and mesoscutellum is continued on the elytron as the elytral shelf, a depressed, shallowly grooved area which receives the posterior edge of the postnotum when the elytra are closed (Doyen 1966).

67. *Elytral base, apex of the subcostal basivenale*: (0) produced (Figs 20A-C, H-L); (1) reduced in length (Figs 20D,E, arrow) (ci: 1.0, ri: 1.0).
68. *Elytral base, anterior margin (in dorsal view)*: (0) not sinuate (Figs 20A-F, H-L); (1) sinuate (Fig. 20G) (ci: 0.50, ri: 0.75).
69. *Elytral base, distance apex of humeral plate to the apex of the subcostal basivenale (in respect to length of anterior margin)*: (0) small (Figs 20D-L); (1) large (Figs 20A,C) (ci: 1.0, ri: 1.0).
70. *Elytral base, anterior margin (dorsal view)*: (0) hook-like elevated (Figs 20H, arrow); (1) convex (Figs 20A,C,G,J,L, arrow); (2) straight or concave (Figs 20D-F,K) (ci: 0.33, ri: 0.80).
71. *Elytral base, radio-medial suture (rms) basally*: (0) moderately curved (Figs 20H,J); (1) almost straight (Figs 20D-G,K); (2) strongly curved (Figs 20A,C,L) (ci: 0.16, ri: 0.58).
72. *Elytral base, anal lobe* (Larsén 1966): (0) completely developed (Figs 20A,B,F,H,J); (1) posteriorly reduced (Fig. 20E) (ci: 1.0, ri: 1.0).

The origin of the anal lobe is difficult to reconstruct, likely it is in main portion derived from the cubital basivenale.

*Hind wing*

73. *Anterior border of ala distal of apical hinge*: (0) glabrous (Fig. 20M); (1) completely setose (Fig. 20T); (2) setose behind apical hinge (Fig. 20N) (ci: 0.28, ri: 0.58).
74. *Wing vein $RA_3$ and $RA_4$ in basal third*: (0) strongly divergent, $RA_4$ in basal third strongly bent (Figs 20O,T); (1) subparallel (Figs 20P-R); (2) weakly divergent, $RA_4$ in basal third weakly bent (Fig. 20S) (ci: 0.66, ri: 0.93).
75. *Wing vein $RA_3$ and $RA_4$ apically*: (0) separate (Figs 20O,Q,S,T); (1) fused or contiguous (Figs 20P,R) (ci: 0.50, ri: 0.90).
76. *Wing vein $RP_1$*: (0) contiguous with $RP_2$ basally (Figs 20O,S); (1) basally reduced, widely separate from $RP_2$ (Figs 20P-R,T) (ci: 0.33, ri: 0.88).
77. *Wing vein $RP_1$ apically*: (0) convergent with $RA_4$ (see Kukalová-Peck and Lawrence 1993, Fig. 52, p. 238); (1) convergent and confluent with $RA_4$ (Figs 20O,P,R-T); (2) subparallel with $RA_4$ (Fig. 20Q) (ci: 1.0, ri: 1.0).
78. *Ratio $RA_3$/ $RA_4$*: (0) distinctly larger than 1.0 (Figs 20O,Q,S); (1) approximately 1.0 (Figs 20P,R,T); (2) little larger than 1.0 (ci: 0.66, ri: 0.90).
79. *Wing, anterior anal vein (AA)*: (0) straight (Fig. 20R); (1) convexly curved or bluntly bent (Figs 20Q,U); (2) acutely bent (Fig. 20O) (ci: 0.50, ri: 0.66).

*Abdomen*

80. *Abdominal sternite seven (penultimate ventrally visible sternite) posteriorly*: (0) with a narrow membrane (Figs 25B,C); (1) with a very broad membrane (Fig. 25A); (2) without membrane (Fig. 25D) (ci: 0.25, ri: 0.45).

The numeration of the abdominal sternites by different authors do not reflect the homology of these segments (e.g. Mikšič 1976; Sanmartin and Martin-Piera 2003) due to the reduction of sclerotization in the basal abdominal segments. Krell (1996) examined the musculature of the ectodermic genitalia and provided clear terminology for the homology of the abdominal segments.

81. *Abdominal sternites ventrally*: (0) separate (Figs 24A, 25A-D); (1) medially fused (Fig. 24B); (2) completely fused (ci: 0.50, ri: 0.33).
82. *Propygidium and sternite seven*: (0) completely separate (Fig. 24C); (1) partially fused at base (Fig. 24D); (2) completely fused (Fig. 24E) (ci: 0.22, ri: 0.50).

*Genitalia (genital segment, both sexes)*

83. *9th tergite*: (0) convex or subrectangular, without any process at basal margin (Fig. 24J); (1) with two processes at basal margin (Fig. 25E) (ci: 1.0, ri: 1.0).

*Male genitalia*

84. *Spiculum gastrale (ventrale), vestigial (9th) sternite*: (0) present (Figs 24F-K); (1) absent (Fig. 24L) (ci: 1.0, ri: 1.0).

As a ventral part of the genital segment, which is derived from the 9th abdominal segment, the spiculum gastrale, consists of a cranial and a caudal portion. The cranial portion is interpreted by Hieke (1966) to be derived from lateroventrally displaced and secondarily cranially fused tergal apodemes IX. The caudal portion, which Sanmartin and Martin-Piera (2003) termed "vestigial sternite", originates presumably from sternite IX (Krell 1996).

The vestigial (9th) sternite is analogously absent or reduced also in some representatives of Rutelinae and Dynastinae, such as *Parastasia* and *Cyclocephala* (Jameson 1998).

85. *Spiculum gastrale, basally widened piece*: (0) at least half as long as wide (Figs 24F-J); (1) considerably shorter than wide (Figs 24K,L) (ci: 0.25, ri: 0.86).
86. *Spiculum gastrale, cranial apex*: (0) not produced (Figs 24F-H); (1) moderately produced (process approximately as long as widened basal portion) (Fig. 24J); (2) strongly produced (process more than twice as long as widened basal portion) (Figs 24K,L) (ci: 0.15, ri: 0.47).

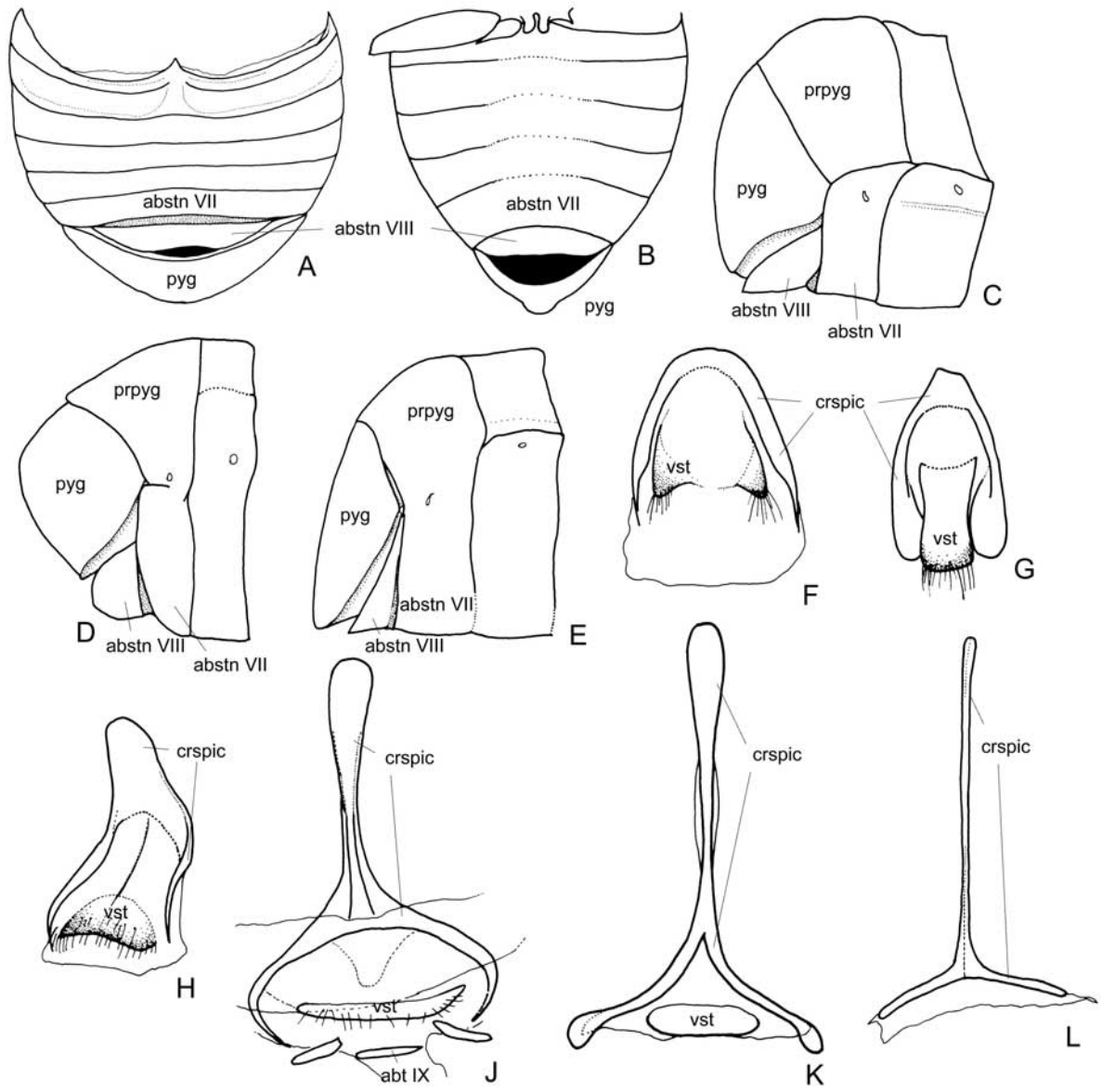


**Fig. 24. A:** abdomen, ventral view: *Oryctes nasicornis*; **B:** abdomen, ventral view: *Melolontha melolontha*; **C:** abdomen, lateral view: *Nepaloserica procera rufescens*; **D:** abdomen, lateral view: *O. nasicornis*; **E:** abdomen, lateral view: *Amphimallon solstitiale*; **F: s**piculum gastrale, ventral view: *Orphnus* sp.; **G: s**piculum gastrale, ventral view: *Hybalus graecus*; **H: s**piculum gastrale, ventral view: *Hoplia graminicola*; **J: s**piculum gastrale, ventral view: *Athlia rustica*; **K: s**piculum gastrale, ventral view: *A. solstitiale*; **L: s**piculum gastrale, ventral view: *Omaloplia ruricola* (not to scale).

87. *Spiculum gastrale, cranial process*: (0) broad and dorsoventrally flattened (Figs 24F-K); (1) throughout filiform, very slender and circular in cross section (Fig. 24L) (ci: 1.0, ri: 1.0).

According to Jameson (1998) character state 1 occurs also in some ruteline genera, such as *Rutela* and *Pelidnota*, however it should be considered as an analogous development to that within the sericine lineages.

88. *Aedeagus, sclerotized plates at apex of ventral phallobase*: (0) absent (Figs 26B-E, M-O); (1) present (Figs 26A,F,L,P-S) (ci: 0.25, ri: 0.84).
89. *Aedeagus, sclerotized plates at apex of ventral phallobase*: (0) separate (Fig. 25F-K,26R); (1) fused with each other (Figs 26L,Q,P); (2) fused with each other and with lateral lamina of phallobase (Fig. 25L) (ci: 0.40, ri: 0.70).

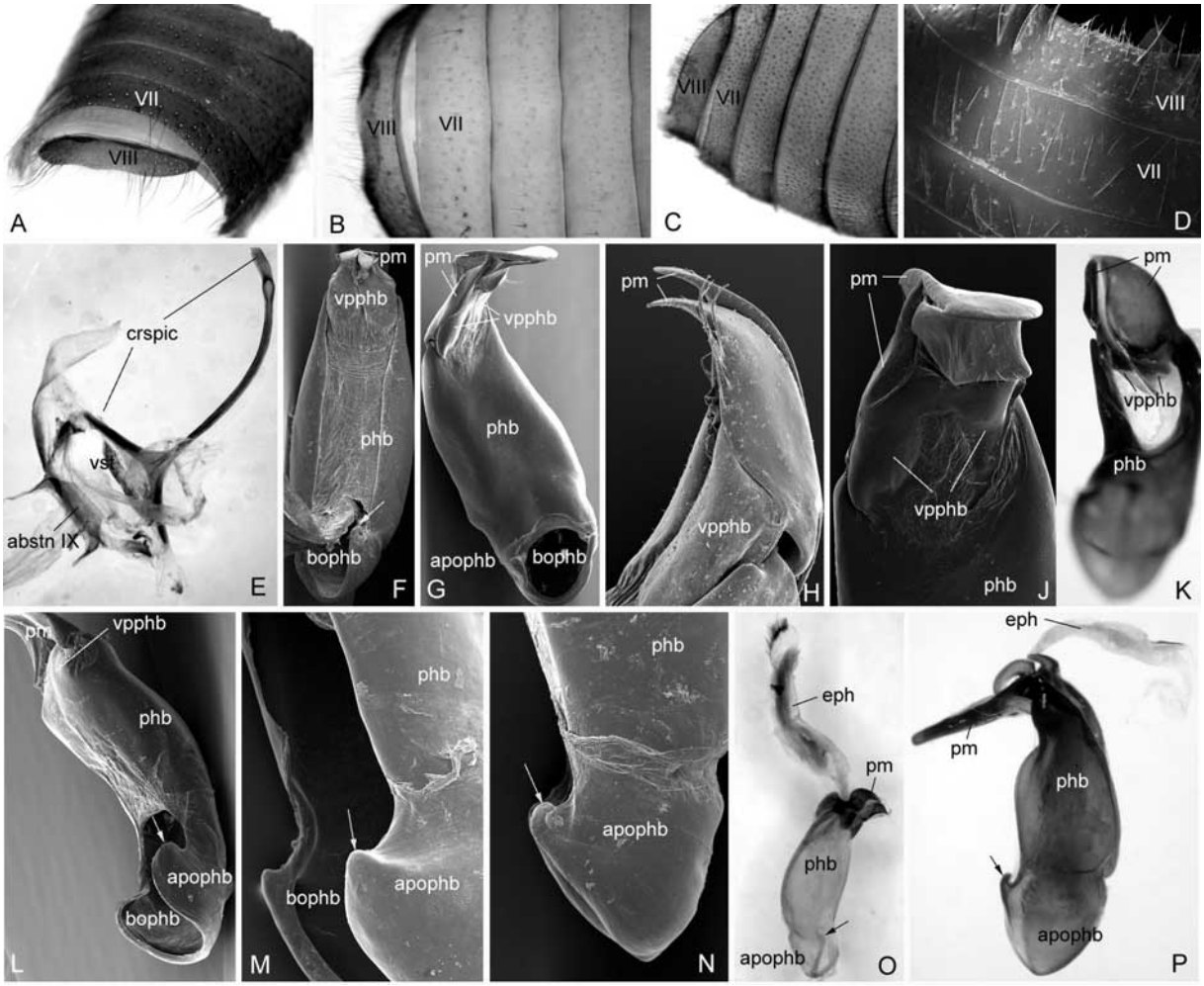


**Fig. 25. A-D:** abdominal sternites; **A, D:** ventral view, **B, C:** medial view; A: *Chasmatopterus hirtus*; C: *Athlia rustica*; **D:** *Cyrtocamenta pygidialis*; **E:** spiculum gastrale, *Camenta westermanni*; **F, G, K:** aedeagus, ventral view; **H:** apex aedeagus, lateral view; **F, H:** *Paratriodonta romana*; **J:** apex aedeagus, lateral view; **G, J:** *Serica pommeranzi*; **B, K:** *Amiserica chiangdaoensis*; **L:** aedeagus, ventrolateral view, *Comaserica bergrothi*; **M:** phallobase, ventrolateral view, *Raysymmela pallipes*; **N:** phallobase, lateral view, *Hymenoplia castilliana*; **O, P:** aedeagus, lateral view; **O:** *Triodontella* sp., **P:** *Nepaloserica schmidti* (not to scale).

90. *Aedeagus, basal ostium of phallobase*: (0) large (at least half as long as phallobase) (Figs 26L-R); (1) small (less than half as long as phallobase) (Figs 25F,G,L, 26G-J,K,S) (ci: 0.33, ri: 0.90).
91. *Phallobase ventrally*: (0) membraneous (Figs 25F, 26M-O,Q,R); (1) sclerotized initiating from lateral lamina of phallobase (Figs 25G,J,L, 26K,S); (2) ventral plates enlarged basally, sclerotized along midline too (Fig. 26P) (ci: 0.28, ri: 0.66).
92. *Phallobase ventrally, lateral lamina at level of distal border of basal ostium*: (0) unarmed or convex (Figs 26B-E); (1) with robust hook-like structure (Figs 25N,P, 26G,S); (2) with blunt tooth (Figs 25L,M, 26F,H,J) (ci: 0.33, ri: 0.78).
93. *Parameres apically*: (0) glabrous (Figs 25J,P, 26B,F,K-P); (1) setose (Figs 25H,O, 26Q) (ci: 0.25, ri: 0.70).
94. *Endophallus, temones*: (0) present (Figs 27A-D, F-H); (1) absent (Fig. 27E) (ci: 0.50, ri: 0).

The temones are a paired, elongate endophallic sclerite articulating to base of median lobe and extending into the basal piece [phallobase] (D'Hotman and Scholtz 1990). Krell (1996) pointed out that in Lamellicornia homologization of endophallic sclerites is far from resolved, consequently he termed the "temones" neutrally as "proximal endophallic sclerite". However, the location in the endophallus seems presently a rather suitable criterion for homology of the endophallic sclerites within Scarabaeidae.

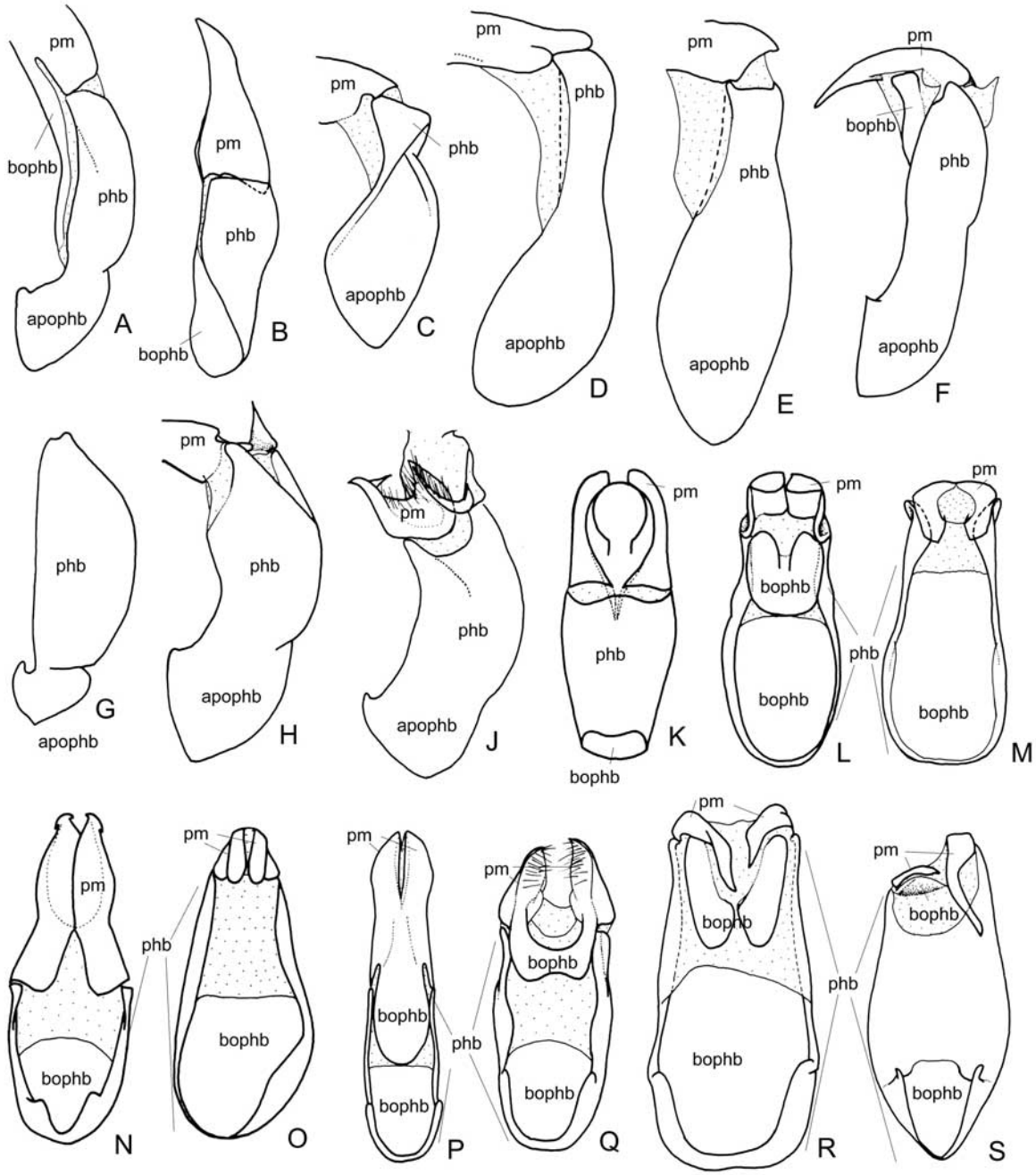


**Fig. 26. A:** Phallobasis, lateral view: *Adoretus* sp.; **B:** Phallobasis, lateral view: *Aphodius* sp.; **C:** Phallobasis, lateral view: *Chasmatopterus hirtus*; **D:** Phallobasis, lateral view: *Elaphocera tangerina*; **E:** Phallobasis, lateral view: *Athlia rustica*; **F:** Phallobasis, lateral view: *Camenta westermanni*; **G:** Phallobasis, lateral view: *Triodontella* sp.; **H:** Phallobasis, lateral view: *Pleophylla* sp.; **J:** Phallobasis, lateral view: *Omaloplia ruricola*; **K:** aedeagus, ventral view: *Trox sabulosus*; **L:** aedeagus, ventral view: *Hybalus graecus*; **M:** aedeagus, ventral view: *Phyllotocus macleayi*; **N:** aedeagus, ventral view: *Melolontha melolontha*; **O:** aedeagus, ventral view: *Elaphocera tangerina*; **P:** aedeagus, ventral view: *Adoretus* sp.; **Q:** aedeagus, ventral view: *Raysymmela pallipes*; **R:** aedeagus, ventral view: *C. westermanni*; **S:** aedeagus, ventral view: *Serica thibetana* (not to scale).

95. *Endophallus, temones*: (0) long and slender (Figs 27A-D,F); (1) short and wide (Figs 27G,H) (ci: 0.25, ri: 0.72).
96. *Endophallus, v-shaped piece*: (0) present and fully developed (Figs 27A-C); (1) absent (Fig. 25O); (2) strongly reduced (Figs 27E,G,H) (ci: 0.33, ri: 0.78).

The term "v-shaped piece" was introduced by Sanmartin and Martin-Piera (2003). It represents the caudal portion of the caudally convergent temones (proximal endophallic sclerite), which is situated ventrally on the endophallus. In Scarabaeidae, the v-shaped piece

may be fused or separated with the cranial portion of the temones, which apically are stretched out to the dorsal face of the endophallus.

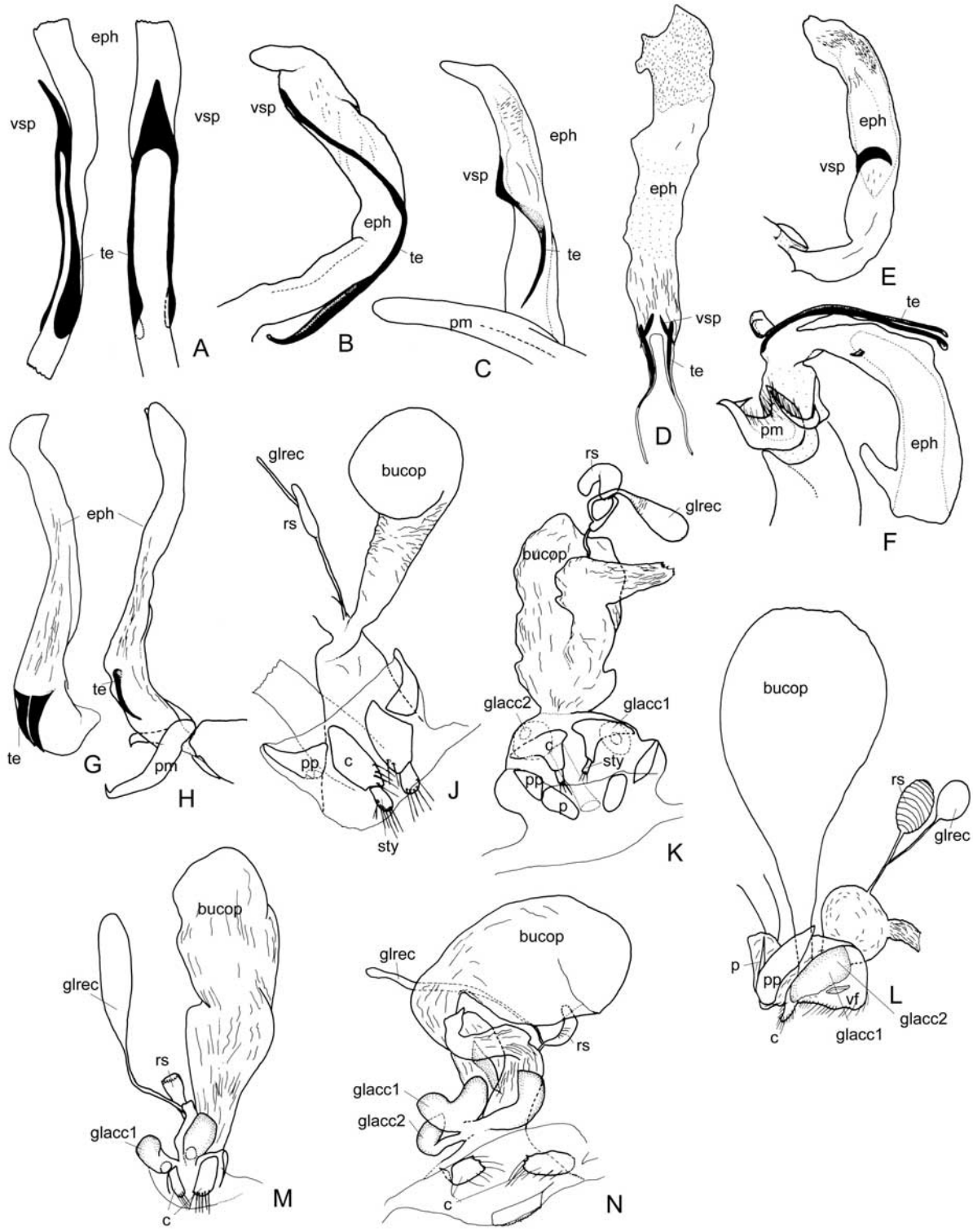


**Fig. 27. A:** endophallus, lateral and ventral view: *Aphodius* sp.; **B:** endophallus, lateral view: *Melolontha melolontha*; **C:** endophallus, lateral view: *Hoplia graminicola*; **D:** endophallus, ventral view: *Elaphocera* sp.; **E:** endophallus, lateral view: *Athlia rustica*; **F:** endophallus, lateral view: *Omaloplia ruricola*; **G:** endophallus, ventral view: *Maladera insanabilis*; **H:** endophallus, lateral view: *M. insanabilis*; **J:** female external genitalia, ventral view:: *Trox sabulosus*; **K:** female external genitalia, ventral view: *Orphnus* sp.; **L:** female external genitalia, lateral view: *Elaphocera capdeboni*; **M:** female external genitalia, ventral view: *Phyllotocus macleayi*; **N:** female external genitalia, ventral view: *Maladera holosericea* (not to scale).

97. *Endophallus, v-shaped piece and temones*: (0) fused (Figs 27A-D,F); (1) separate (Figs 27D,F-H) (ci: 0.12, ri: 0.41).

*Female genitalia*

98. *Glandulae accessoriae*: (0) absent (Figs 27J,K); (1) present (Figs 27L-N); (2) secondarily reduced (uninformative).

Since the monophyly of *Aphodius* + *Copris* has been shown in several studies by a number of apomorphies (e.g. Browne and Scholtz 1998), I have coded the loss of the accessory glands in Scarabaeinae, represented herein by *Copris*, as a independent character state to retain a higher tree resolution.

99. *True styli*: (0) present (Figs 27J,K); (1) absent (Figs 27L-N) (ci: 0.50, ri: 0).

According to Tanner (1927) the styli are not homologous to the so called "genital palps" (or vaginal palps, e.g. Krell 1996) as suggested Sanmartin and Martin-Piera (2003), the latter are derived from coxite of the 9th segment. Holloway (1972) presented a hypothesis that the styli including their basal hemisternites (e.g. in Trogidae and Lucanidae) are derived from the 10th segment; however, she provided no evidence for this assumption. According to the studies of Tanner (1927) the following sclerites and their respective terminology used in some later works are homologous (e.g. Coca-Abia and Martin-Piera 1991; Sanmartin and Martin-Piera 2003): proctiger (= vestigial tergite 1), paraproct (= vestigial tergite 2), valvifer (= vestigial sternite).

100. *Sclerotized portion of valvifer*: (0) present (Figs 27J-L); (1) absent (Figs 27M,N) (ci: 0.20, ri: 0.77).
101. *Glandulae accessoriae*: (0) left and right glandulae separately lead to the vagina (Figs 27L,M); (1) left and right glandulae with a common duct leading to the vagina (Fig. 27N) (ci: 1.0, ri: 1.0).
102. *Membraneous anal fold between 8th and 9th segment (ventral view)*: (0) large [enclosing the glandulae accessoriae if present] (Figs 27J-L); (1) small or absent leaving the glandulae accessoriae free (Figs 27M,N) (ci: 0.20, ri: 0.75).

*Larva*

103. *Galea*: (0) with two joints (Fig. 28A); (1) with one joint (Figs 28B-D) (uninformative).
104. *Haptomerum (epipharynx), number of heli*: (0) three or four (Fig. 28E); (1) more than five (Figs 28G,H); (2) less than two (Fig. 28F) (ci: 0.28, ri: 0.58).
105. *Galea and lacinia*: (0) entirely separate (Figs 28A,B); (1) fused but with a complete suture (suture may be absent basally) (Fig. 28C); (2) entirely fused, without suture (Fig. 28D) (ci: 1.0, ri: 1.0).
106. *Anal split*: (0) y-shaped, medially deeply incised (Figs 28J,M,O,Q); (1) medially moderately incised (Fig. 28N); (2) medially not incised (Figs 28K,L,P) (ci: 0.40, ri: 0.75).
107. *Palidium (last sternite)*: (0) absent (Figs 28J,K,L,M); (1) transverse and arched (Figs 28Q); (2) transverse and angled (Fig. 28O); (3) longitudinal and straight (one row of setae) (Figs 28N,P) (ci: 0.50, ri: 0.50).

The palidium is part of a raster on last abdominal sternite of larvae. Cribb et al. (1998) revealed that this raster is a complex of mechanoreceptive setae. Their chemical and morphological investigations did not provide any evidence that the raster is a site for chemical emissions. The ultrastructure of the setae of palidium (pali) have shown that each seta is innervated by a single dendrite that ends in a tubular body at the base of the seta. Due to the limited number of taxa examined by Cribb et al. (1998), there is no indication, how the pali differ from normal setae of ventral surface of last abdominal sternite, and whether the pali within the diverse phytophagous lineages are truly homologous.

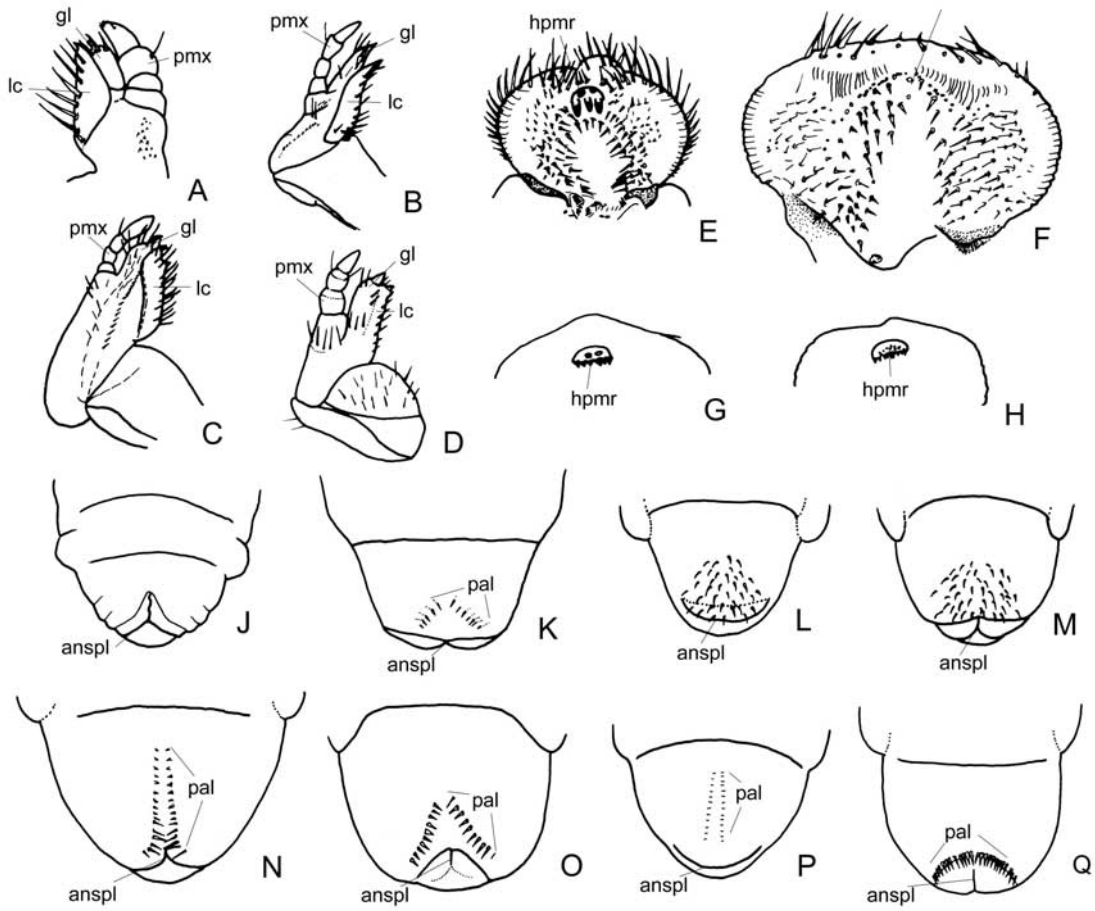


**Fig. 28. A:** maxilla, dorsal view: *Trox scaber*; **B:** maxilla, dorsal view: *Aphodius hamatus*; **C:** maxilla, dorsal view: *Maladera castanea*; **D:** maxilla, dorsal view: *Cetonia aurata*; **E:** epipharynx, ventral view: *Serica ligulata*; **F:** epipharynx, ventral view: *Propomacrus mucronatus*; **G:** haptomerum (epipharynx), ventral view: *Heteronyx* sp.; **H:** haptomerum (epipharynx), ventral view: *Adoretus sinicus*; **J:** larva, raster: *Trox unistriatus*; **K:** larva, raster: *Aphodius pardalis*; **L:** larva, raster: *A. sinicus*; **M:** larva, raster: *Hoplia equina*; **N:** larva, raster: *Amphimallon majalis*; **O:** larva, raster: *Heteronyx* sp.; **P:** larva, raster: *Anomala orientalis*; **Q:** larva, raster: *M. castanea* (not to scale).

## Results

The analysis of 107 adult and larval characters with the parsimony ratchet and the above mentioned settings yielded 109 equally parsimonious trees of 426 steps (CI: 0.36, RI: 0.76). Repeating the search ten times I obtained the same statistics as above. Characters 98 and 103 were uninformative in the present data set. The strict consensus of these trees, with jackknife values and Bremer support, is presented in Fig. 29 with areas of topological conflict shown as polytomies. Repeating the parsimony ratchet with modified settings (1000 iterations and ten trees hold per iteration with ten sequential ratchet runs) resulted in an increasing number of equally parsimonious trees without an altered topology in the strict consensus tree. The tree topology was not affected by altering ACCTRAN or DELTRAN optimizations.

In some cases data for the characters of thoracic musculature and of larval morphology were missing. To test the sensitivity of the results to missing data, additional analyses have been run: one omitting characters 42 to 45, which resulted in no alteration of consensus topology of the full analysis, and a second deleting characters 42 to 45 and 103 to 107 from the analysis. These analyses were run using the same settings for the parsimony ratchet and yielded 90 equally parsimonious trees of 399 steps (CI: 0.35, RI: 0.76).

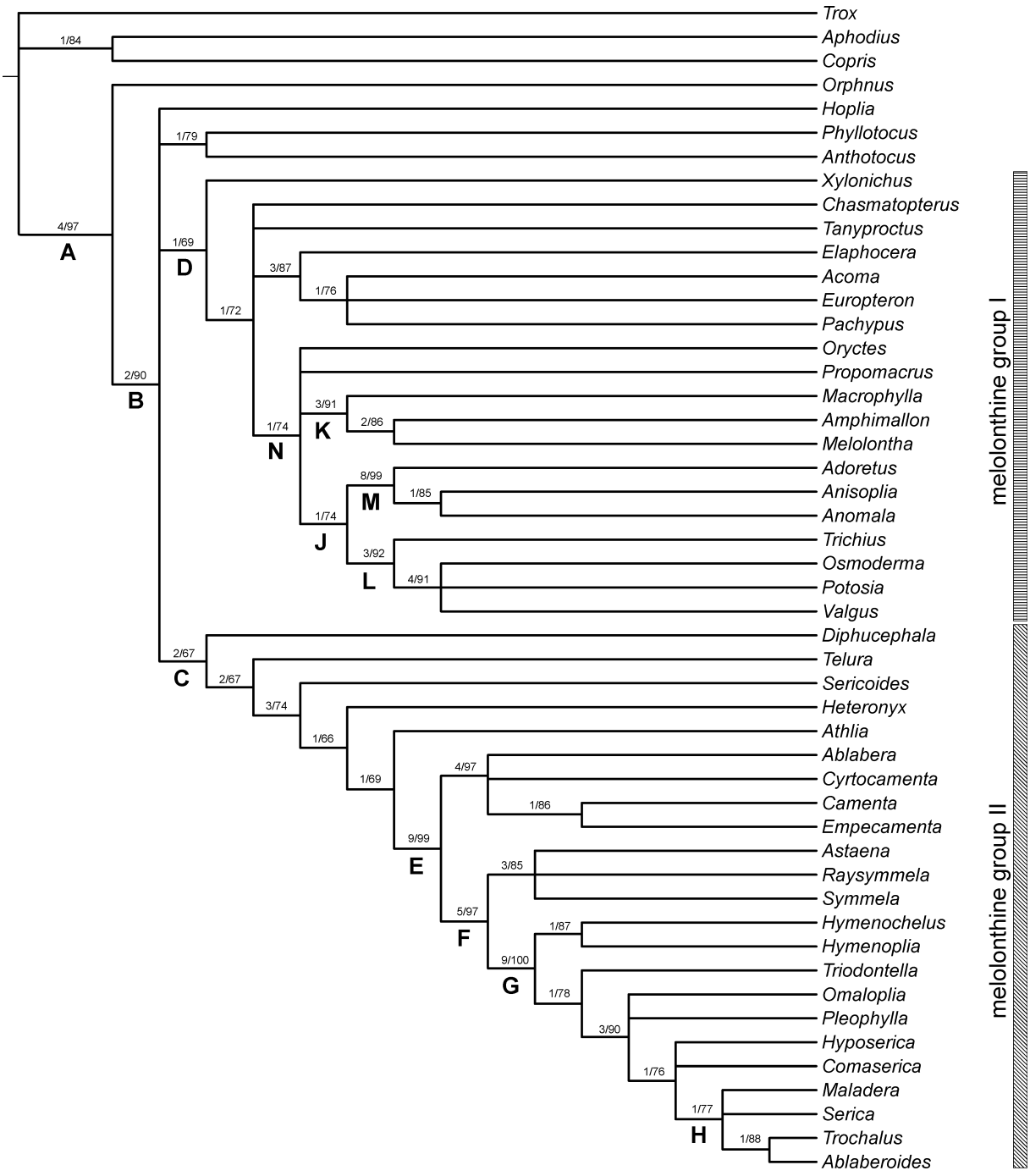


**Fig. 29.** Strict consensus of 109 equally parsimonious trees with a length of 426 steps (CI: 0.36 and RI: 0.76); above each branch support indices (Bremer support/ jackknife values).

The strict consensus (Fig. 30) shows a similar topology to the consensus tree of the first analysis (Fig. 29) with all characters included. The position of a few taxa was different, including Phyllotocini (*Phyllotocus* + *Anthotocus*) and *Diphucephala*, and the clade comprising *Aphodius* + *Copris* was no longer monophyletic. Since data on the larval morphology were available for most principal lineages, and the alteration of the topology excluding larval characters was minimal, further discussion will be based only on the full character analysis. Figure 31 illustrates unambiguous character changes along each branch of the consensus tree from the first analysis (with all characters included), which was used for the following discussion of the apomorphies and the character evolution of groups and lineages.

The strict consensus tree (Fig. 29) reveals six major clades: (1) the 'aphodiine line' (Browne and Scholtz 1998) including *Aphodius* + *Copris*; (2) the orphnine clade here containing *Orphnus*; (3) *Hoplia*; (4) Phyllotocini including *Phyllotocus* + *Anthotocus*; (5) the 'melolonthine group I' (node D, Fig. 29) including *Acoma*, *Amphimallon*, *Chasmatopterus*, *Elaphocera*, *Europteron*, *Macrophylla*, *Melolontha*, *Pachypus*, *Propomacrus*, *Tanyproctus*, *Xylonichus*, and the 'ruteline subgroup' of (Browne and Scholtz 1998) represented by *Oryctes*, *Adoretus*, *Anisoplia*, *Anomala*, *Trichius*, *Osmoderma*, *Potosia*, and *Valgus*; as well as (6) the 'melolonthine group II' (node C, Fig. 29) containing *Athlia*, *Diphucephala*, *Heteronyx*, *Sericoides*, *Telura*, Ablaberini, and Sericini.

## Discussion

### *Monophyly of 'orphnine group' + 'melolonthine group'*

The results strongly support the monophyly of the 'orphnine group' + 'melolonthine group'. Both clades were also found to form a monophyletic clade by Browne and Scholtz (1998). In this study monophyly of these groups is based on five non-homoplasious apomorphies (Fig. 31, node A): (1) a short and straight dorsal process (p1) of the mesofurcal arm (31:1); (2) the mesofurcal arm with an the apically narrowed dorsal process (p1) (32:1); (3) metacoxa basally widened with the posterior margin produced posteriorly at the base (52:1); (4) haptomerum of the epipharynx (larvae) with three or four heli (104:0); (5) galea and lacinia of the larvae fused (at least partially) (105:1).

This sister group relationship of the 'orphnine group' and the 'melolonthine group' provides an interesting case of a high asymmetry in species diversity within Scarabaeoidea. While the 'orphnine group' (Orphninae) represents a small group with a few genera and species, the 'melolonthine group' is the lineage with greatest species diversity within the Scarabaeoidea, containing tens of thousands of species. Most taxa in this lineage feed on Angiosperms (Scholtz and Chown 1995).

### *Monophyly of the 'melolonthine group'*

This clade (node B; Bremer support: 2, jackknife: 90%) is based at least on five apomorphies (Fig. 31): (1) galea with one joint (9:1); (2) the distally shortened lacinia not extending beyond the basis of the galea (12:1); (3) the palpiger enclosed by the prementum and the ligular lobe (18:1); (4) wing vein $RA_3$ and $RA_4$ in the basal third strongly divergent with $RA_4$ strongly bent caudally in the basal third (74:0); (5) the large basal ostium of the phallobase at least half as long as phallobase (90:0). The latter character is reversed in Sericini and the representatives of Rutelinae included into this analysis when the basal ostium of the phallobase is small similar to the outgroup (*Trox*) and to the basal lineages (*Aphodius* + *Copris*). I consider the small or lacking incision between caudal lobes of the postnotum (metathorax, 38:1) a less suitable character (ci: 0.25) to support the clade since its development might depend on the specimen's weight and size, although it evolves independently from the size of the postnotal lobes (character 37). The 'melolonthine group' is comprised in the tree by two major melolonthine clades (nodes C and D, Fig. 29).

### *Monophyly of Sericini*

The results of this cladistic analysis support the monophyly of the Sericini. At node F (Bremer support: 5, jackknife: 97%) the following non-homoplasious apomorphies support

the monophyly of this clade: (1) vestigial (9th) sternite in the spiculum gastrale absent (84:1); (2) cranial process of the spiculum gastrale filiform, very slender and circular in cross section (87:1); (3) glandulae accessoriae with left and right glandulae (1+2) having a common duct to the vagina (101:1). The small basal ostium of phallobase (90:1, character reversal from node A) and the enlarged metacoxa (46:1) are important apomorphies of the Sericini. The latter character state is also found in *Phyllotocus*, a genus often placed among the Sericini (e.g. Britton 1957; Dalla Torre 1912; Houston and Weir 1992; Machatschke 1959).

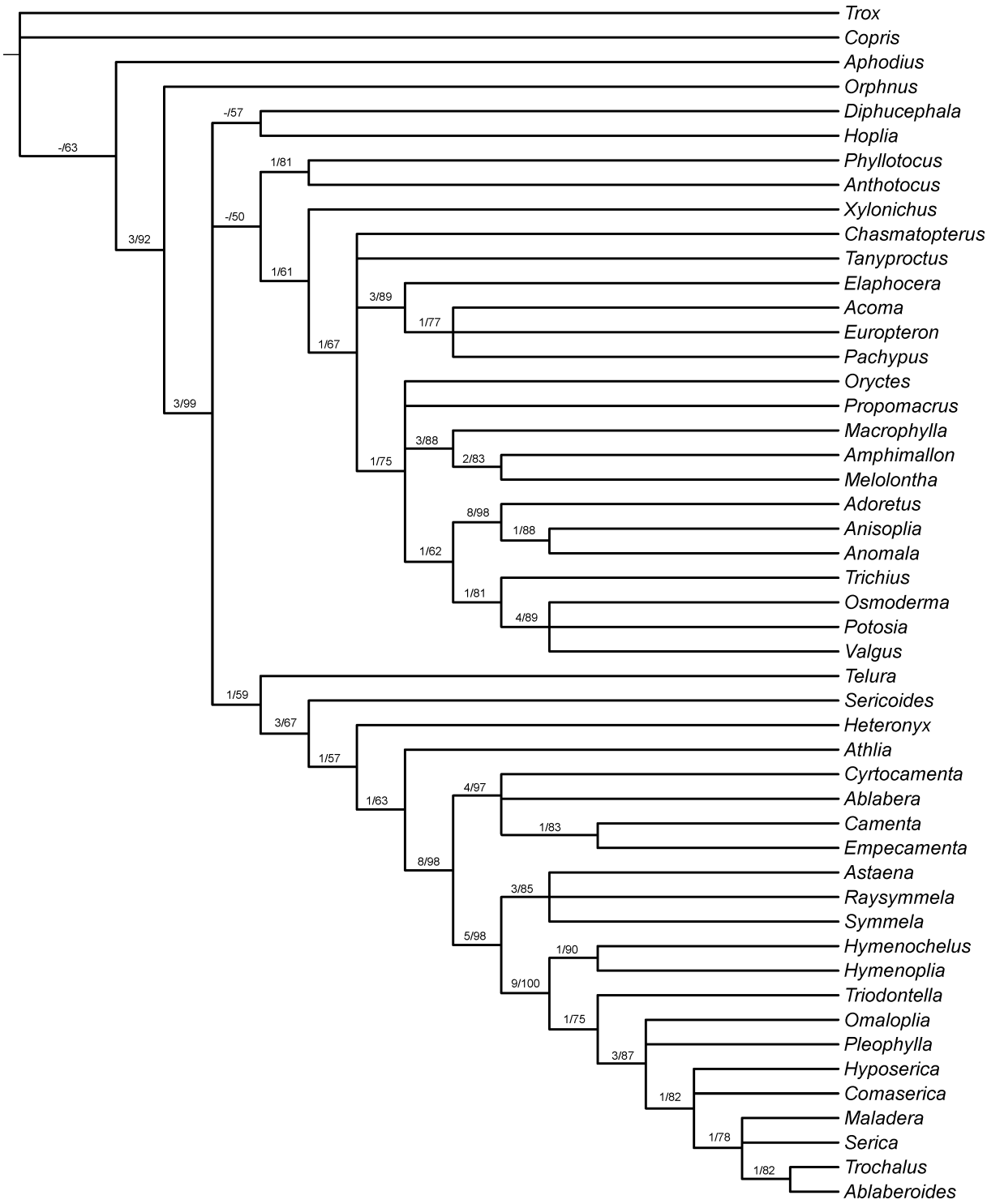


**Fig. 30.** Strict consensus of 90 equally parsimonious trees with a length of 399 steps (CI: 0.35 and RI: 0.76), with characters of thoracic musculature (characters 42 - 45) and larval morphology (characters 103 - 107) excluded from analysis; above each branch support indices (Bremer support/ jackknife values).

*Monophyly of Sericini + Ablaberini*

In concordance with Machatschke (1959) this analysis identified Ablaberini as the sister to Sericini. The monophyly of Sericini + Ablaberini is supported by one non-homoplasious apomorphy: the 9th tergite having two sharply pointed processes at its cranial margin (83:1). The node (E) is also supported by at least eight further apomorphies (Bremer support: 9, jackknife: 99%), such as the completely fused labrum and clypeus (1:1) having a common continuous lateral margin (2:1), the galea having eight teeth (6:2) of which four are visible in ventral view (on maxilla) (10:0), the absence of the marginal line of the posterior margin of the metacoxa (55:0), the basally widened piece of the spiculum gastrale which is considerably shorter than wide (85:1), the present sclerotized plates at the apex of the ventral phallobase of the aedeagus (88:1, the lateral lamina of the ventral phallobase at level of the distal border of the basal ostium with the blunt tooth (92:2), and with apically setose parameres (93:1).

*Evaluation of clades within 'melolonthine group I'*

The 'melolonthine group I' shares several apomorphies at node D, with only one being non-homoplasious (40:1). The included taxa of Melolonthini (node K), Cetoniinae (node L) and Rutelinae (node M) are strongly supported as being monophyletic. However as in Sanmartin and Martin-Piera (2003; e.g. *Sparrmannia*), some of the taxa, (e.g. *Macrophylla*) classified as Pachydemini (Lacroix 2000; Dalla Torre 1912), are placed by this analysis with the genera of Melolonthini. The relationships of Dynastinae (*Oryctes*) and Euchirinae (*Propomacrus*) were not sufficiently resolved with the data matrix used in this analysis. The topology of the clade of 'melolonthine group I' is surprising with the nesting of the Melolonthini (*Macrophylla* (*Amphimallon*, *Melolontha*)) within the 'ruteline subgroup' (Browne and Scholtz 1998) (node N), which is supported by two important apomorphies: (1) the apically fused or contiguous $RA_3$ and $RA_4$ (75:1) and (2) by equally long $RA_3$ and $RA_4$ (ratio $RA_3$/ $RA_4$ approximately 1.0) (for further details consult Fig. 31). Interestingly, *Chasmatopterus* (Chasmatopterini) and *Pachypus* (Pachypodinae) are grouped closely with representatives of Pachydemini (*Tanyproctus*, *Elaphocera*, *Europteron*). In 93% of the maximum parsimonious trees this clade is the sister group (see Fig. 32) of the 'ruteline subgroup'. In the phylogeny of Browne and Scholtz (1998), Dynastinae (represented in this analysis by *Oryctes*) + Rutelinae (*Adoretus* (*Anisoplia*, *Anomala*)) is monophyletic, which is supported by a number of synapomorphies in the hind wing articulation. This close relationship was not seen in the results of this analysis. Since characters used in this analysis were chosen to reconstruct the phylogeny of Sericini, the relationships of the taxa outside this clade should be regarded as preliminary as they may change with the insertion of more characters appropriate for investigating relationships among these taxa.

*Phylogenetic position and evolution of Sericini*

The Sericini + Ablaberini are nested within a clade of taxa with a distribution primarily in southern continents (here so far preliminary termed 'melolonthine group II'). This clade is supported by a small number of apomorphies (node C; 6:4, 7:0, 37:1, 107:1, Fig. 31). The closest relatives of Sericini + Ablaberini are *Athlia* (southern South America) and *Heteronyx* (Australia) (Britton 2000) which have the following apomorphies: (1) all teeth completely fused with the galea (7:1) and (2) meso- and metatarsal claws with a basal or median tooth ventrally (62:1). From the pectinate structure of the topology of this clade one could assume that Sericini + Ablaberini are derived from one of these southern lineages. This hypothesis is consistent with the idea of several authors classifying the Australian and southern American melolonthine lineages into separate tribe taxa (Diphucephalini, Scitalini, Sericoidini,

Heteronycini; cfr. Britton 1957; Houston and Weir 1992; Evans 2003). Since these lineages do not occur in the Paleotropics or Nearctic, it is plausible that the ancestors of Sericini + Ablaberini and *Athlia* were separated by a vicariance event, such as the separation from Gondwana and the northern drift of the African plate, where Sericini and Ablaberini very likely diversified during early Tertiary, with a dispersal of the most basal Sericini over the Atlantic to South America. Similar dispersals are hypothesized and well documented in other groups of animals, such as primates or rodents (e.g. Simpson 1980, Takai et al. 2000).

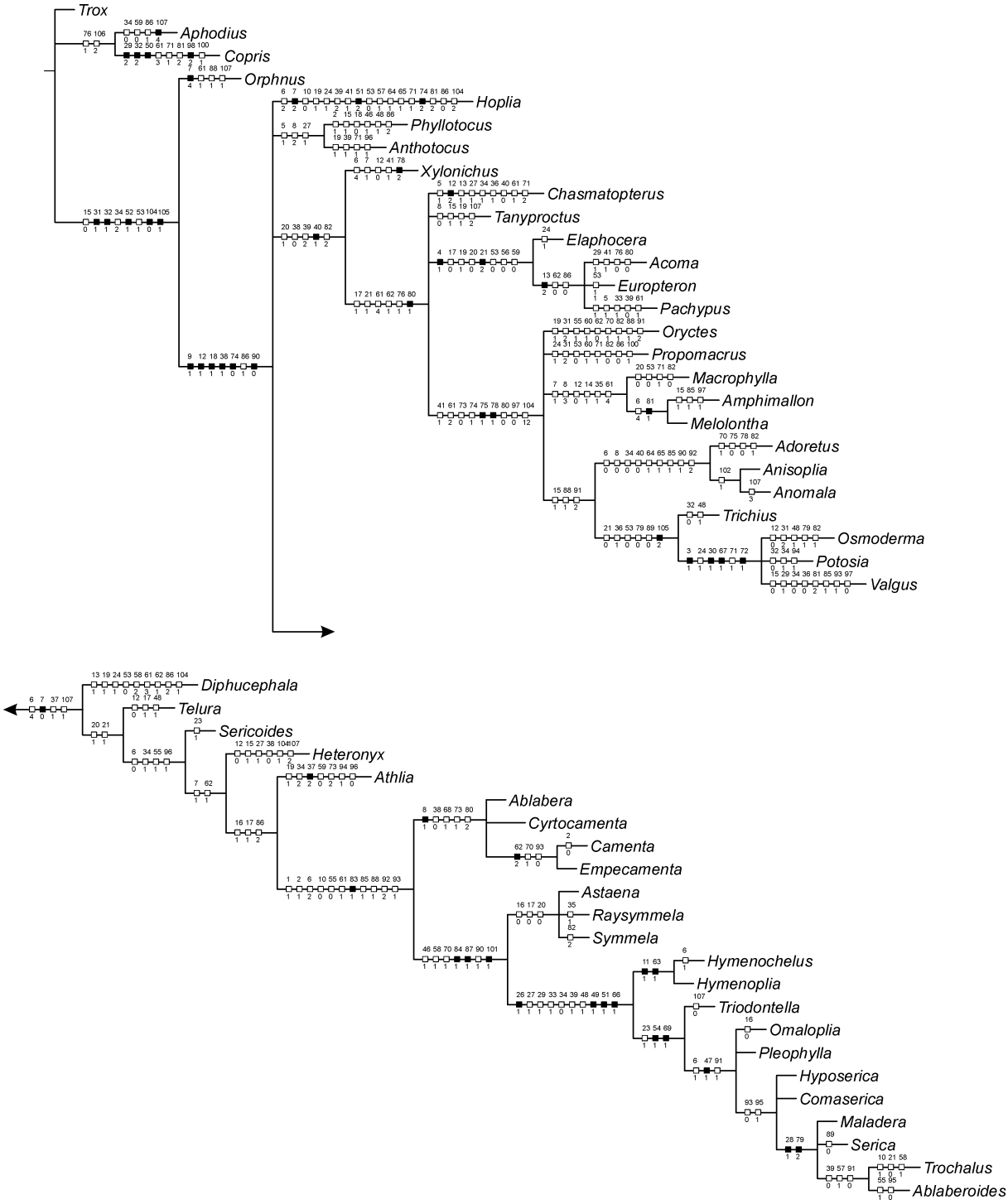


**Fig. 31.** Strict consensus of 107 equally parsimonious trees with a length of 425 steps (CI: 0.36 and RI: 0.76) showing character changes and apomorphies mapped by state (only discontinuous states are mapped as homoplasy and only unambiguous changes are shown, unsupported nodes collapsed and using proportional branch lengths). (full squares: non-homoplasious character states; empty squares: homoplasious character states).

The clade containing *Astaena*, *Raysymmela*, and *Symmela* was restricted to the tropical South America and moved north into Central America (as far as Nicaragua) during the late Tertiary. The monophyly of Holarctic - Palaeotropical Sericini (node G; Bremer support: 9, jackknife: 100%) is best supported by numerous unambiguous apomorphies, such as (1) a large interior process (p3) of the mesofurcal arm (26:1); which is (2) lobiform in shape (34:0); (3) the medially separate mesofurcal arms (27:1); (4) the small and conical craniomedial surface of mesofurcal arm (19:1); (5) the absence of an anterior process (p2) of mesofurcal arm (33:1); (6) the evenly divergent anterior and posterior margin of the ventral median flange of the metendosternite (lateral view) (39:1); (7) the absence of a procoxal transversal carina (48:1); (8) the wide fusion of the proexopleura and trochantin (49:1); (9) the apex of mesotibia with one reduced principal spine (51:1); and (10) the elytral shelf being on the same level as the elytral surface (66:1). Evidence for a radiation of this clade on the African plate includes the fact that most extant basal lineages (*Triodontella*, *Hymenoplia*, *Pleophylla*, *Omaloplia*) of the Holarctic - Palaeotropical Sericini (node G) presently occur just in the Afrotropical and the western Mediterranean region, while the more apical lineages (node H) also occur in Asia and North America (*Maladera*, *Serica*). These 'modern' Sericini share some important unambiguous apomorphies, such as the presence of a carina from the craniolateral margin of the mesosternum to the mesofurcal arm (28:1) and the acutely bent anterior anal vein (AA) (79:2).

It is very difficult to place the oldest known fossils of melolonthine lineages into this phylogeny, since it is impossible to accurately score most of the characters used. In case of the Lower Cretaceous fossil genus *Lithanomala* (Nikolaev 1998), it only has one diagnostic character (the position and shape of the labrum + clypeus), which could place it in at least two vastly different positions in the phylogenetic tree. Similarly, *Cretoserica* (Nikolaev 1998; Krell 2000) has at least four alternative positions throughout the 'melolonthine group' clade. According to the fossil record, the more derived sericine lineages, such as "*Serica*" and "*Maladera*" from North America and Central Europe can be dated to at least the Oligocene using fossils (Krell 2000), which corresponds with the evolutionary hypothesis of Sericini formulated above. For a more detailed biogeographical analysis, it will be necessary to explore the Sericini phylogeny in the context of the role of Madagascar and the Indian plate in the evolution of the group, and consequently to consider a wider range of the more than 200 described sericine genera.

### *Considerations for the classification of melolonthine lineages*

The reconstructed phylogeny of the melolonthine lineages, have implications for the present scarabaeoid classification. According to the consensus tree (Fig. 29), the Melolonthinae (or Melolonthidae, cfr. e.g. Baraud 1992; Lacroix 2000) in its current form (including all taxa of node B, excluding those of node N, but including those taxa united in node K, e.g. Evans 2003) is paraphyletic. This would also be consistent with the difficulty in finding apomorphies for this group (Browne and Scholtz 1998). The results of the analysis (Fig. 29) support the paraphyly of the tribe Pachydemini. Sanmartin and Martin-Piera (2003), also discovered that the monophyly of Pachydemini is not well supported. The representatives of Chasmatopterini (*Chasmatopterus*) and Pachypodinae (*Pachypus*) are nested within the Pachydemini and the node of *Chasmatopterus*, *Tanyproctus*, (*Elaphocera* (*Acoma*, *Europteron*, *Pachypus*)) collapsed to a polytomy that included the 'melolonthine group I' in the strict consensus tree (Fig. 29). Consequently, it appears that Pachydemini should be redefined, once a more robust phylogenetic analysis has been performed on this tribe. Regarding the "Sericinae", I refrain from expanding the term for a wider range of lineages than Sericini + Ablaberini as some authors do (e.g. Britton 1957, Lacroix 2000), because

some of the these relationships need further detailed studies before they can be persistently applied to the classification of the group.

Regarding the exclusion of *Athlia* from Sericini, it is premature to erect a new tribe for this genus until more detailed studies are done to explore the relationships between southern hemispheric melolonthine lineages.

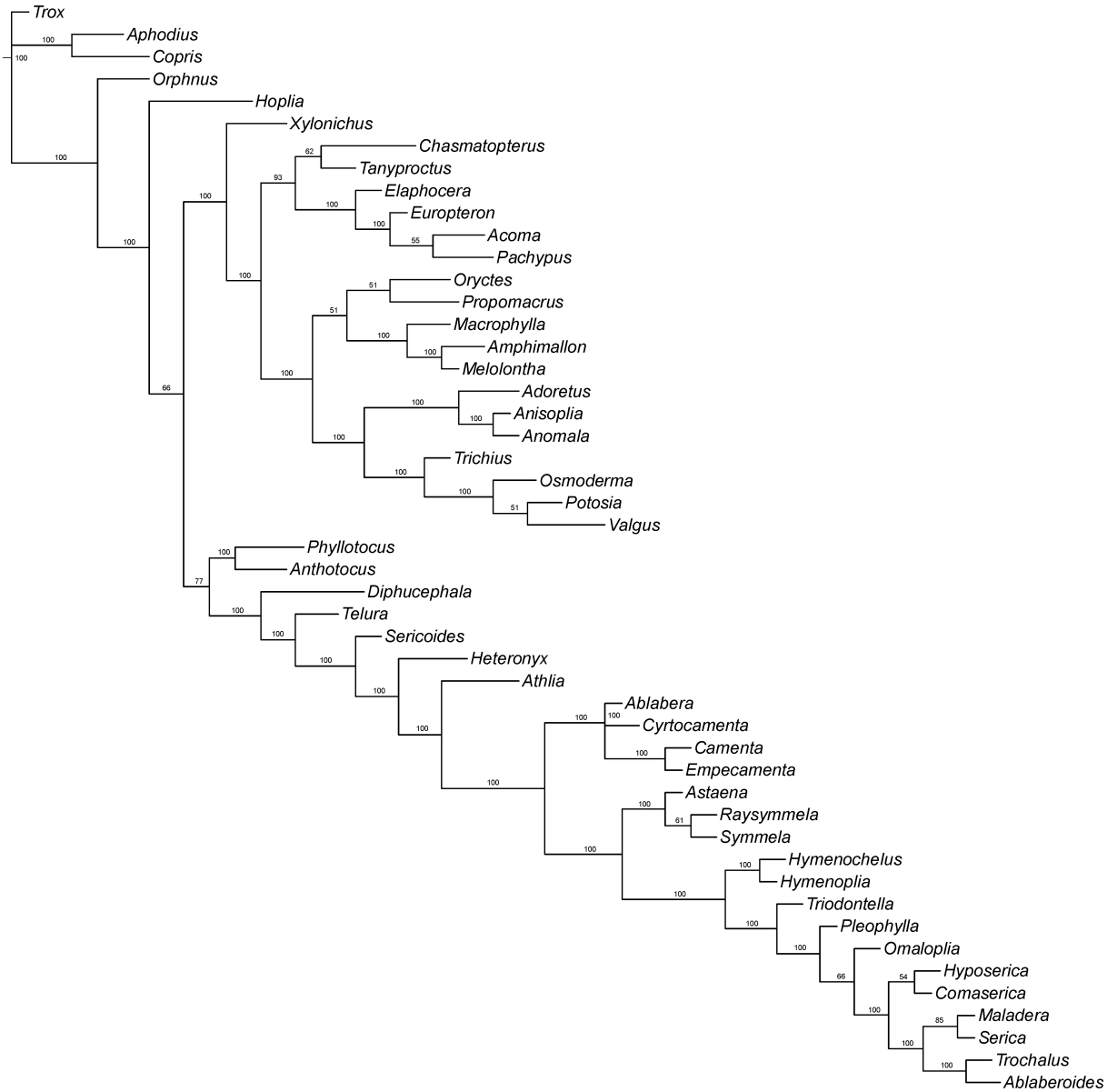


**Fig. 32.** Majority rule consensus tree generated with WINCLADA showing unsupported nodes collapsed and using the proportional branch lengths. The numbers above the branches indicate the frequency of the node among all maximum parsimonious trees.